Propylene and Butylene Glycol: New Alternatives to Ethylene Glycol in Conjugated Polymers for Bioelectronic Applications

Maximilian Moser,*[,†,a] Yazhou Wang,*[,†,b] Tania Cecilia Hidalgo,[†,c] Hailiang Liao,[b] Yaping Yu,[b] Junxin Chen,[b] Jiayao Duan,[b] Floriana Moruzzi,[a] Sophie Griggs,[a] Adam Marks,[a] Nicola Gasparini,[d] Andrew Wadsworth,[a] Sahika Inal,[*,c] Iain McCulloch[a,e] and Wan Yue*[,b]

[a]University of Oxford, Department of Chemistry, Oxford, OX1 3TA, United Kingdom

[b]State Key Laboratory of Optoelectronic Materials and Technologies, Key Laboratory for Polymeric Composite and Functional Materials of the Ministry of Education, School of Materials and Engineering, Guangzhou Key Laboratory of Flexible Electronic Materials and Wearable Devices, Sun Yat-Sen University, Guangzhou, 510275, China

[c]King Abdullah University of Science and Technology (KAUST), Biological and Environmental Science and Engineering (BESE), Organic Bioelectronics Laboratory, Thuwal, 23955-6900, Saudi Arabia

[d]Imperial College London, Department of Chemistry and Centre for Plastic Electronics, London, W12 0BZ, United Kingdom

[e]King Abdullah University of Science and Technology (KAUST), Physical Science and Engineering Division, Thuwal, 23955-6900, Saudi Arabia

[†]These authors contributed equally.

Table of Contents

1. General Methods

Materials: Solvents of spectroscopic grade were purchased from Sigma Aldrich and used as received. Synthetic intermediates and final monomers were purified by column chromatography using silica gel (General-Reagent, 200-300 mesh) unless otherwise stated. Polymers were purified by sequential Soxhlet extractions in various solvents.

NMR Spectroscopy: ^{1}H and ^{13}C{^{1}H} NMR spectra were recorded in $CDCl_3$ or 1,1,2,2-tetrachloroethane-d_2 (TCE-d_2) with a Bruker Avance III spectrometer (400 or 500 MHz for ^{1}H and 101 MHz for ^{13}C{^{1}H}). Chemical shifts (δ) are reported in parts per million (ppm) downfield from tetramethylsilane (TMS) and are referenced using residual chloroform (δ_H = 7.26 ppm and δ_C = 77.2 ppm) or 1,1,2,2-tetrachloroethane (δ_H = 6.00 ppm and δ_C = 73.8 ppm) as internal standard. Coupling constants (J) are given in Hertz (Hz) and multiplicities are indicated as singlet (s), doublet (d), triplet (t), or multiplet (m).

Gel Permeation Chromatography (GPC): GPC was recorded on a Shimadzu RID-20A-LC-20AD-CTO-20AC machine calibrated against a set of narrow dispersity polystyrene standards. GPC was conducted at 40 °C, employing $CHCl_3$ as the eluent.

UV-Vis Absorption Spectroscopy: UV-Vis absorption spectra were measured with an Agilent Technologies (Cary 5000/6000i) Cary Win UV-Vis spectrophotometer. Solution UV-Vis spectra were recorded in $CHCl_3$ at a concentration of $1.0 \cdot 10^{-5}$ M in a quartz cuvette with a 1 cm pathlength. Thin film polymer samples were prepared by spin-coating 5 mg mL^{-1} polymer $CHCl_3$ solutions onto ITO-coated glass substrates.

Cyclic Voltammetry: CV measurements were carried out using a Shanghai Chenhua Instrument CHI760E potentiostat with a three-electrode set-up. An Ag/AgCl couple was used as the reference electrode, a Pt wire as the counter electrode, and a polymer-coated glassy carbon electrode as the working electrode. Polymer thin film samples were prepared analogously to those used for UV-Vis absorption spectroscopy. Measurements were carried out either in an organic or aqueous-based electrolyte. The organic electrolyte consisted of a 0.1 M tetrabutylammonium hexafluorophosphate (TBA PF_6) solution in anhydrous acetonitrile. For CV measurements in the organic electrolyte, the ferrocene/ferrocenium couple (Fc/Fc$^+$) was used as an internal standard. Aqueous CV measurements were instead conducted in a 0.1 M aqueous sodium chloride solution.

Ionisation potentials (*IP*) were determined according to **Equation 1**.[1]

$$IP\ (eV) = \left(5.1 + E_{ox,org} - E_{Fc/Fc^+}\right) \qquad \textbf{Equation 1}$$

where $E_{ox,org}$ is the semiconductor's onset of oxidation in a 0.1 M solution of TBA PF_6 in acetonitrile and E_{Fc/Fc^+} is the half-wave potential of the ferrocene/ferrocenium (Fc/Fc$^+$) couple in a 0.1 M solution of TBA PF_6 in acetonitrile.

Spectroelectrochemistry: Spectroelectrochemical measurements were performed by fitting the CV setup inside the UV-Vis absorption spectrophotometer. Potentials were applied for 15 s prior recording the UV-Vis absorption spectrum at each voltage to ensure stabilisation of the optical trace. Potential steps of 0.1 V were then used to evaluate the electrochromic behaviour of the polymers. All spectroelectrochemical measurements were conducted using a 0.1 M aqueous sodium chloride solution as the supporting electrolyte.

Atomic Force Microscopy (AFM): AFM measurements were performed in tapping mode, using a Bruker Dimension Icon AFM with a silicon tip. Pristine polymer thin film samples were prepared analogously to those used for UV-Vis absorption spectroscopy. Hydrated polymer samples were prepared by immersing the pristine polymer films into a 0.1 M aqueous sodium chloride solution for 1 h followed by drying under a stream of nitrogen prior recording the AFM images. AFM images of electrochemically cycled polymer films were subsequently obtained by using the hydrated polymer films as the working electrode in CV measurements and cycling the films for 50 cycles. Films were then washed with deionised water and dried with nitrogen before recording their images.

Grazing-incidence Wide-angle X-ray Scattering (GIWAXS): Samples for X-ray scattering were prepared analogously to those used for UV-Vis absorption spectroscopy albeit using native oxide silicon wafers as the substrates. An incidence angle of 0.18° and a photon energy of 8 keV were used to record the scattering patterns.

Electrochemical Quartz Crystal Microbalance with Dissipation (eQCM-D): Swelling measurements were done using Ti/Au-coated quartz crystals (QSensors QSX 338), the QSense

Electrochemistry Module (QEM 401), and the QSense Analyzer (Biolin Scientific). First frequency (*f*) and dissipation (*D*) shifts (1st – 11th harmonics) of the bare sensors were recorded in both air and an aqueous 0.1 M NaCl solution. Immersion of the sensors into the liquid electrolyte causes a shift in signals, arising from the density and mass changes inside the chamber, which need to be considered for changes in the polymers upon electrolyte exposure. After signal stabilisation, the sensors were removed from the analyser, spin-coated with the polymer under evaluation, and placed back in the module. Frequency and dissipation signals were recorded for the Ti/Au/polymer sensors until signal stabilisation, in air and in NaCl 0.1 M, as done for the bare sensors. Using the "Stitch Data Files" function within the QSoft software we obtained the shifts in f and D signals before and after the sensor was coated, for both dry and wet states. These differences were used to calculate the mass changes (Δm) on the crystal, using the Sauerbrey equation:

$$\Delta m =- 17.7 \cdot \frac{\Delta f}{n}$$ **Equation 2**

where Δf is the frequency shift and n is the overtone number.

eQCM-D was performed by coupling an Autolab PGSTAT128N to the QSense EC Module. The employed three-electrode setup comprised an Ag/AgCl reference electrode, a Pt counter electrode, and the polymer-coated QSX 338 as the working electrode. We used the composite Sauerbrey model in the DFind software was used to estimate acquired mass of the films during electrochemical biasing. It was suggested that the relationship between the dissipation and frequency change is below a certain threshold ($\Delta D_n/(-\Delta f_n/n) \ll 4 \times 10^{-7}$ Hz^{-1}), Sauerbrey equation can be applied.[2] This model uses a weighted average of all harmonics and applies equation 2 to derive the mass. We used 4 harmonics for our analysis. To calculate the anion density injected into the films during doping/dedoping processes, we assumed that each hole couples with one anion (Cl- for NaCl solution). We estimated the number of anions by calculating the charge that is measured at a given doping voltage and multiplying it by the elementary charge ($1.602176634 \times 10^{-19}$ C). This value can be verified with Faraday's law of electrolysis, as shown in Equation 3.

$$m = \frac{Q * M_{Cl}}{F * n}$$ **Equation 3**

where m is the mass of the injected Cl^- ions, Q is the charge accumulating on the working electrode, M_{Cl-} is the atomic mass of Cl^-, F is the Faraday constant, and n is the valence number of Cl^- (i.e., 1). Since there is more mass that the film gains, that cannot be accounted by the anion mass taken up, we attribute the remaining mass to water. To find the water that the film takes up, we subtracted the calculated mass of Cl^- anions from the total mass that the film acquires during electrochemical doping. Finally, to calculate the number of water molecules, we divided this value with the mass of one water molecule mass ($2.99158 \cdot 10^{-23}$ g atom^{-1}). Areal normalisation was done by dividing the mass changes over the sensor's active area ($A = \pi * (0.5\ cm)^2$, while thickness estimations were obtained by dividing areal mass over film density (1000 g/L).

Swelling percentages were calculated using:

$$\%\ Swelling_{total} = \frac{Volume_{wet\ at\ x\ V} - Volume_{dry}}{Volume_{dry}} \cdot 100 \qquad \textbf{Equation 4}$$

OECT and microelectrode array fabrication: Organic electrochemical transistors were fabricated based on a previous protocol using the sacrificial peel-off method. In summary, glass wafers were patterned with a positive photoresist (S1813) followed by Cr/Au magnetron sputtering. After lift-off in organic solvent, contacts were insulated by a parylene C layer, vaporized on the substrates with an adhesion promoter. An anti-adhesion layer was applied before vaporizing the second parylene C layer, used as a sacrificial layer for semiconductor patterning. The source-drain contacts were patterned using a thick photoresist (AZ9260) and subsequently etched using oxygen plasma. The same technique was used to generate gold patterns of various geometries, which were then coated and patterned with the polymers. The width of the OECT channels was 100 µm while the length was 6 µm, giving a W/L ratio of ~16.67. The polymers were spin-casted onto the substrates from polymer solutions in $CHCl_3$ with a concentration of 5 mg mL^{-1} in. Film thickness in the channel was determined using AFM.

T characterization: OECTs were characterized using a Keithley 2602B dual-channel SMU operated by custom LabView programmes. We obtained the bandwidth data using a NI-PXIe unit. We performed all measurements using 0.1 M aqueous NaCl solution as the electrolyte and an Ag/AgCl pellet (2x2 mm, Warner Instruments) as the gate electrode. For bandwidth measurements, we applied a constant drain voltage (-0.6 V for p(g2T-TT) and -0.65 V for p(p2T-TT) and p(b2T-TT)) and a gate voltage resulting in $g_{m,max}$. The voltage modulation at the gate electrode was generated using sinusoidal pulses with amplitude of 10 mV varying in a frequency range of 1 to 20,000 Hz.

2. Synthetic Procedures

2.1 Synthesis of the Side Chains

S1, **S2**, **S4**, and **S5** were synthesised according to the literature.[3,4]

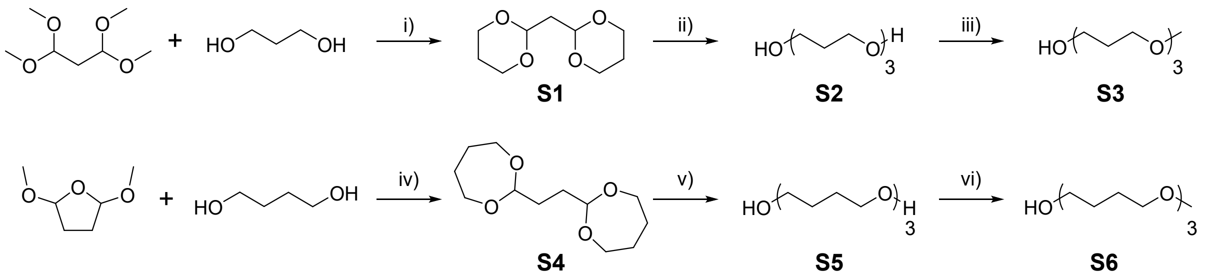

Scheme S1 Synthesis of the side chains **S3** and **S6**. (i) pTsOH (cat.), toluene, 110 °C; (ii) BH_3-THF (2.5 equiv.), THF, 0 °C then 60 °C; (iii) NaH (1.0 equiv.), CH_3I (1.0 equiv.), THF, 0 °C then RT; (iv) pTsOH (cat.), CH_2Cl_2, 40 °C; (v) BH_3-THF (2.5 equiv.), THF, 0 °C then 60 °C; (vi) NaH (1.0 equiv.), CH_3I (1.0 equiv.), THF, 0 °C then RT.

Synthesis of S3

S2 (5.00 g, 26.0 mmol, 1.00 equiv.) was dissolved in THF (26 mL). A dispersion of sodium hydride in mineral oil (1.04 g, 26.0 mmol, 1.00 equiv.) was added to the mixture at 0 °C and allowed to warm to room temperature over 40 min while stirring. After that, methyl iodide (3.69 g, 26.0 mmol, 1.00 equiv.) was added dropwise to the reaction mixture at 0 °C followed by overnight stirring. The reaction was quenched by addition of distilled water. The aqueous phase was extracted with dichloromethane and the combined organic layers were washed with water and brine before being dried over anhydrous sodium sulfate. Excess solvent was removed under reduced pressure. The crude product was purified by silica flash column chromatography to give **S3** as a yellow oil (3.21 g, 15.6 mmol, 60% yield).

^{1}H NMR (400 MHz, CDCl$_3$, 300 K) *δ*: 3.77 (q, *J* = 4.9 Hz, 2H), 3.61 (t, *J* = 5.7 Hz, 2H), 3.54 – 3.44 (m, 8H), 3.33 (s, 3H), 1.88 – 1.76 (m, 6H).

^{13}C{^{1}H} NMR (101 MHz, CDCl$_3$, 300 K) *δ*: 70.3, 69.7, 68.3, 67.8, 67.7, 62.2, 58.6, 32.0, 30.0, 29.9.

HRMS (ESI): *m/z* calculated for $C_{10}H_{22}O_4$: 206.1518, [M+H]$^+$ found: 207.1570.

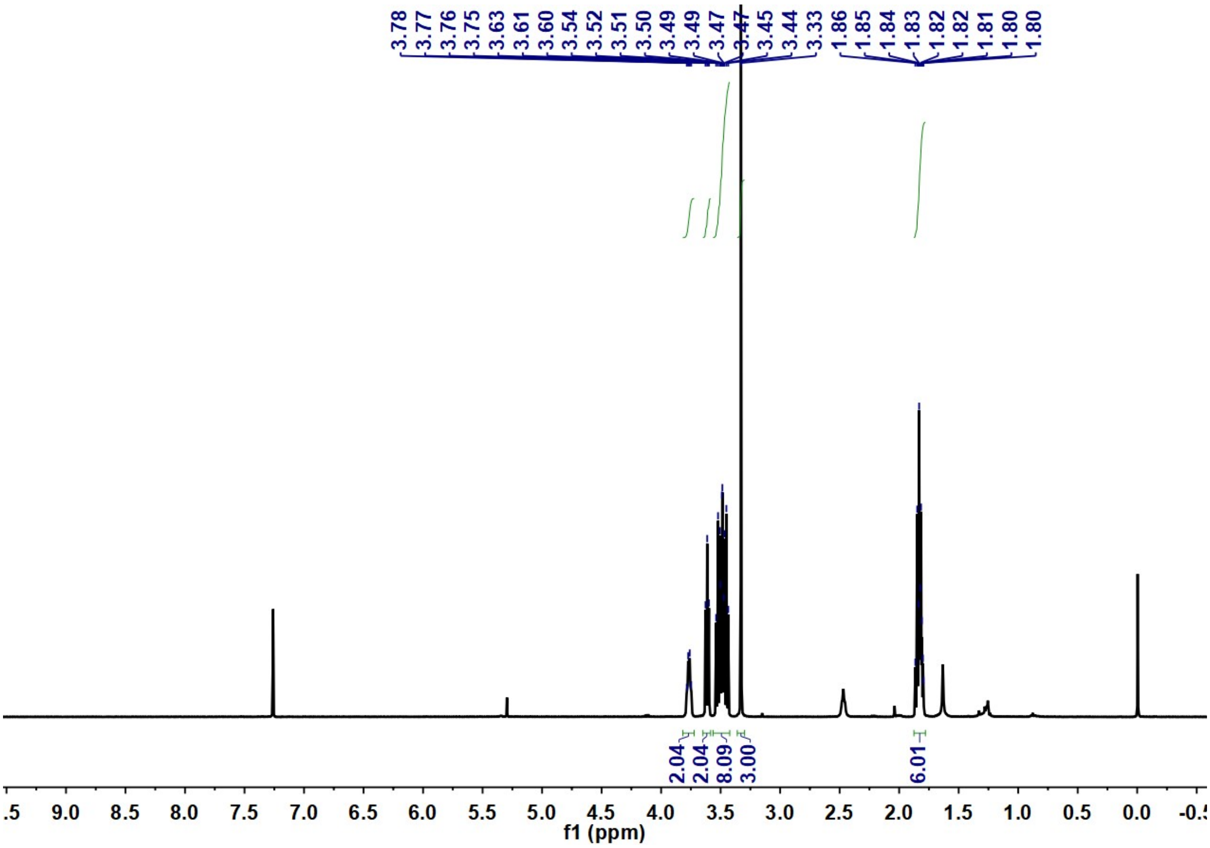

Fig S1 ^{1}H NMR spectrum of **S3**.

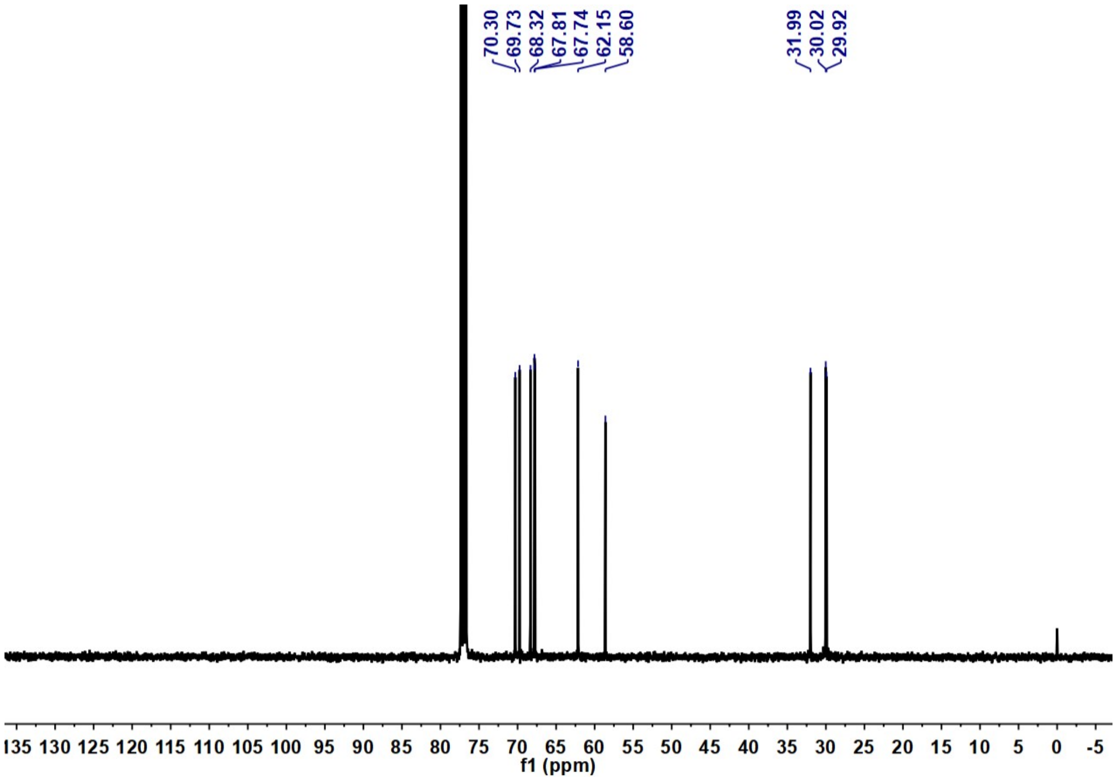

Fig S2 $^{13}C\{^1H\}$ NMR spectrum of **S3**.

Synthesis of S6

S5 (5.00 g, 21.4 mmol, 1.00 equiv.) was dissolved in THF (22 mL). A dispersion of sodium hydride in mineral oil (0.85 g, 21.4 mmol, 1.00 equiv.) was added to the mixture at 0 °C and allowed to warm to room temperature over 40 min while stirring. After that, methyl iodide (3.03 g, 21.4 mmol, 1.00 equiv.) was added dropwise to the reaction mixture at 0 °C followed by overnight stirring. The reaction was quenched by addition of distilled water. The aqueous phase was extracted with dichloromethane and the combined organic layers were washed with water and brine before being dried over anhydrous sodium sulfate. Excess solvent was removed under reduced pressure. The crude product was purified by silica flash column chromatography to give **S6** as a yellow oil (3.71 g, 15.0 mmol, 70% yield).

^1H NMR (400 MHz, $CDCl_3$, 300 K) δ: 3.64 (t, J = 5.8 Hz, 2H), 3.52 – 3.35 (m, 10H), 3.33 (s, 3H), 1.74 – 1.54 (m, 12H).

$^{13}C\{^1H\}$ NMR (101 MHz, $CDCl_3$, 300 K) δ: 72.6, 70.9, 70.6, 70.5, 62.8, 58.5, 30.4, 27.0, 26.5, 26.4, 26.4, 26.4.

HRMS (ESI): *m/z* calculated for $C_{13}H_{28}O_4$: 248.1988, $[M+H]^+$ found: 249.2062.

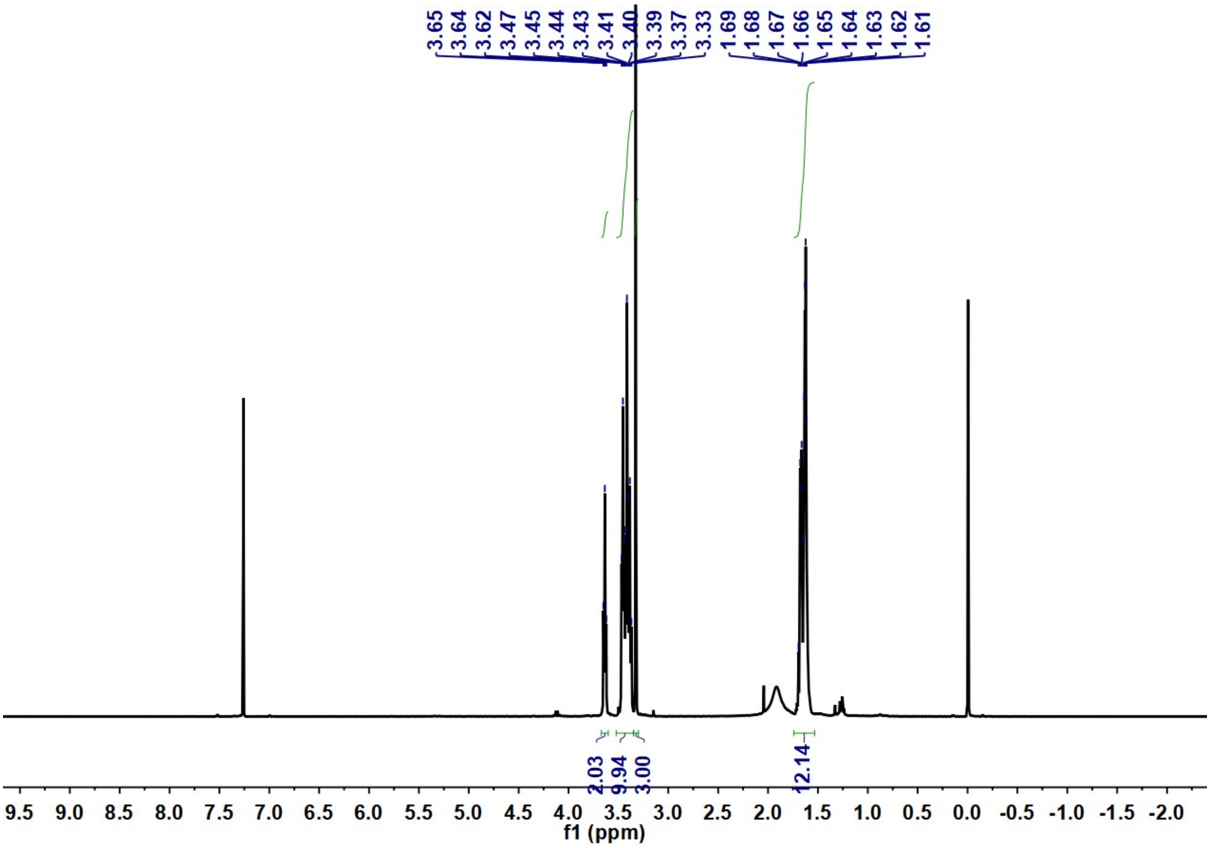

Fig S3 ^{1}H NMR spectrum of **S6**.

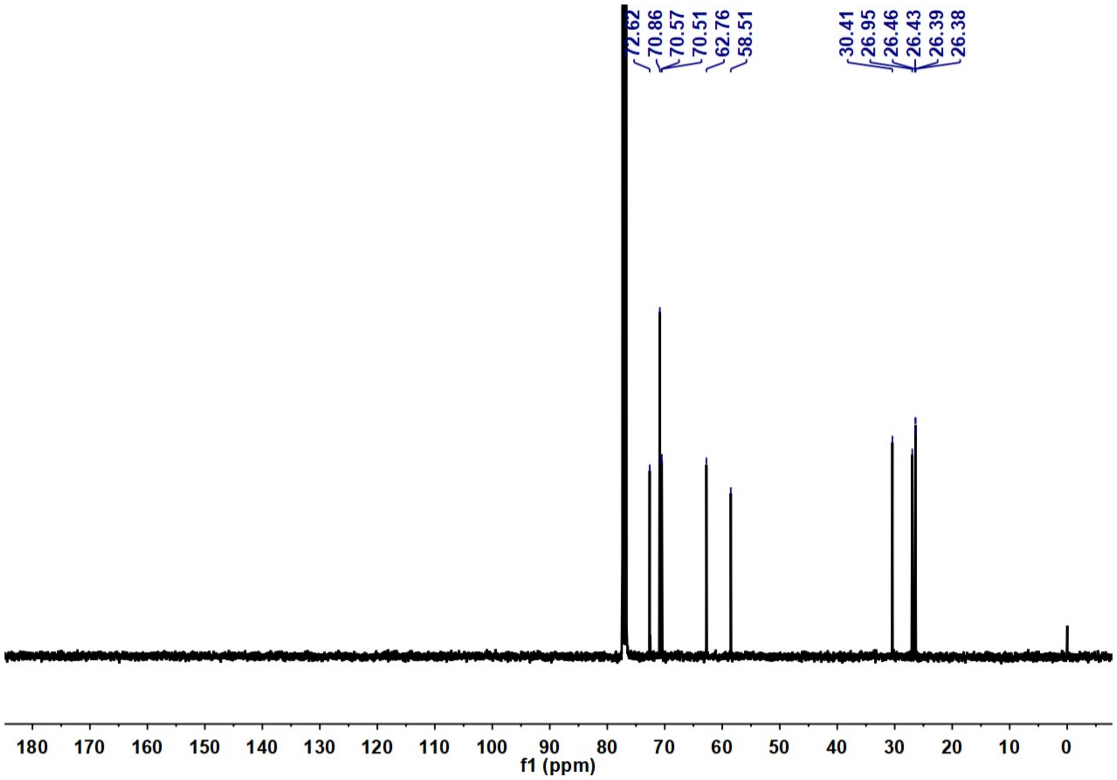

Fig S4 $^{13}C\{^1H\}$ NMR spectrum of **S6**.

2.2 Monomer Synthesis

S7a, **S8a**, **S9a**, and **S10a** were synthesised according to the literature.[5]

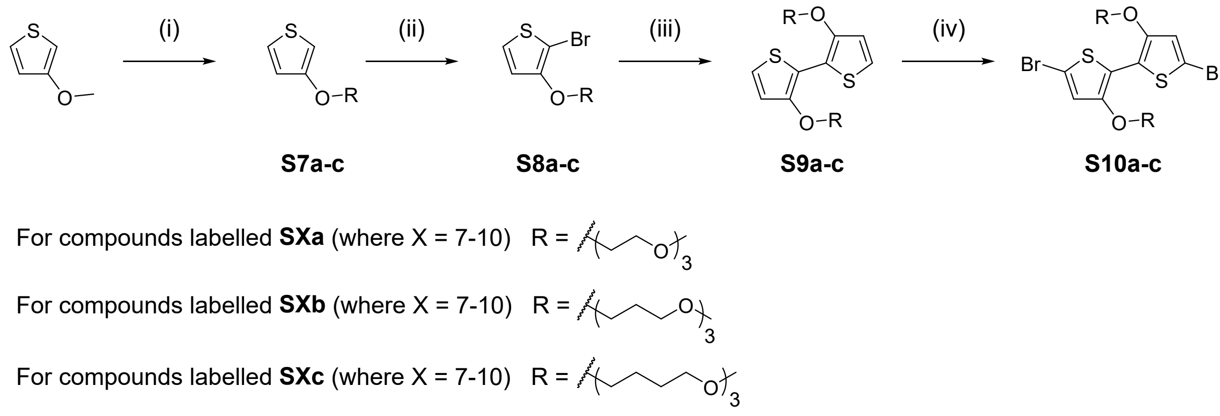

Scheme S2 Synthesis of the bromide functionalised bithiophene monomers **S10a-c**. (i) ROH (2.0 equiv.), pTsOH (cat.), toluene, 110 °C; (ii) NBS (1.0 equiv.), THF/hexane, 0 °C; (iii) $Ni(COD)_2$ (2.0 equiv.), COD (1.0 equiv.), BPy (1.2 equiv.), THF, RT then 66 °C; (iv) NBS (2.0 equiv.), $CHCl_3$, 0 °C.

Synthesis of S7a-c

S7a: 3-methoxythiophene (15.00 g, 131.3 mmol, 1.00 equiv.), triethylene glycol monomethyl ether (42.95 g, 261.6 mmol, 1.991 equiv.), and *p*-toluenesulfonic acid monohydrate (2.49 g, 13.1 mmol, 0.100 equiv.) were dissolved in toluene (500 mL) and the resulting mixture heated to reflux for 6 h. After cooling the reaction to room temperature, the solvent was removed under reduced pressure. The crude product was purified by silica flash column chromatography to afford **S7a** as a pale-yellow oil (13.62 g, 55.35 mmol, 42% yield).

S7b and **S7c** were synthesised analogously to **S7a**.

S7b was obtained as a pale-yellow oil (2.32 g, 8.04 mmol, 50% yield).

^{1}H NMR (400 MHz, $CDCl_3$, 300 K), δ: 7.16 (dd, *J* = 5.2, 3.1 Hz, 1H), 6.74 (dd, *J* = 5.2, 1.1 Hz, 1H), 6.25 (dd, *J* = 2.8, 1.3 Hz, 1H), 4.04 (t, *J* = 6.3 Hz, 2H), 3.57 (t, *J* = 6.2 Hz, 2H), 3.53 – 3.42 (m, 8H), 3.32 (s, 3H), 2.06 – 2.01 (m, 2H), 1.87 – 1.78 (m, 4H).

^{13}C{^{1}H} NMR (101 MHz, $CDCl_3$, 300 K) δ: 157.9, 124.6, 119.5, 97.2, 69.8, 67.9, 67.8, 67.3, 67.1, 58.6, 30.0, 30.0, 29.7.

HRMS (ESI): *m/z* calculated for $C_{14}H_{24}O_4S$: 288.1395, $[M+H]^+$ found: 289.1468.

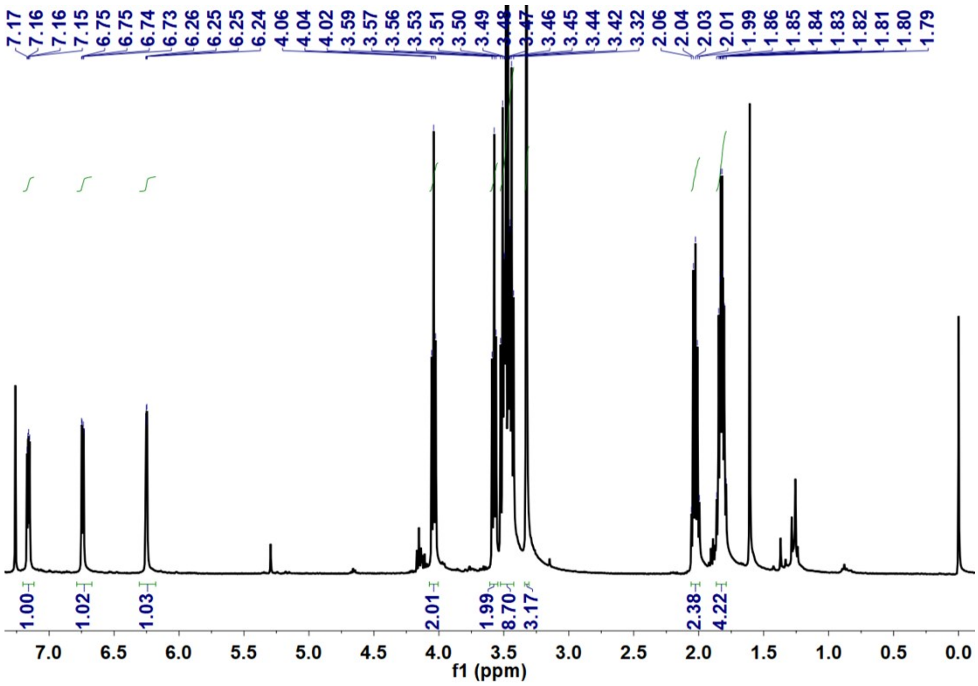

Fig S5 ^{1}H NMR spectrum of **S7b**.

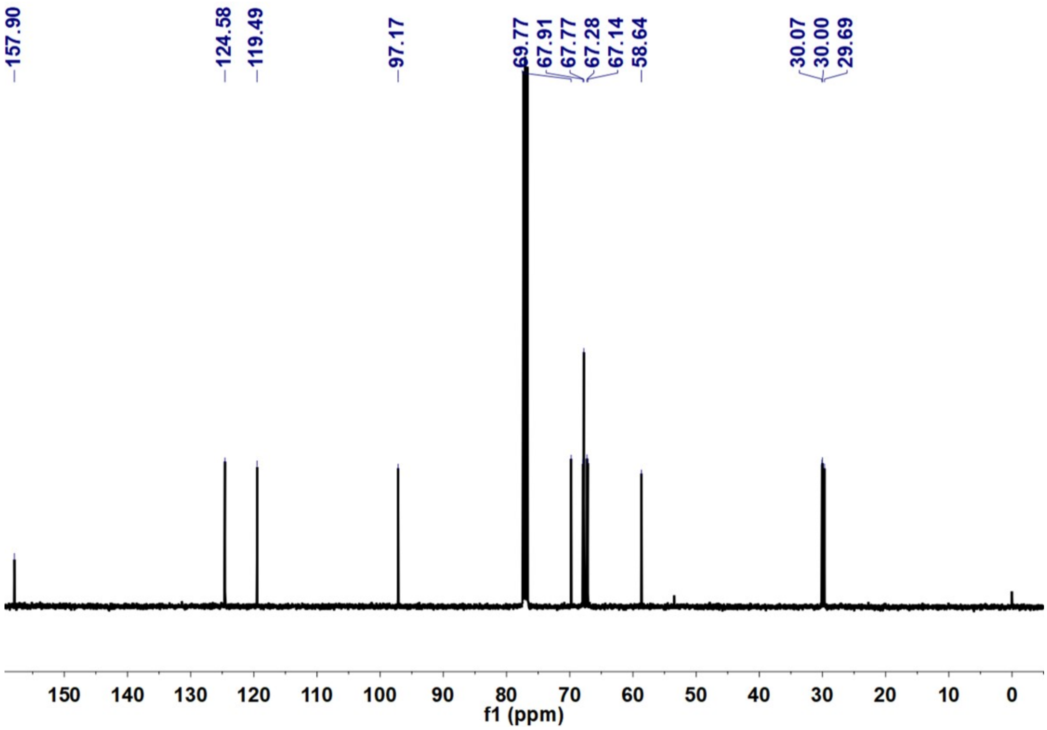

Fig S6 ^{13}C{^{1}H} NMR spectrum of **S7b**.

S7c: **S7c** was obtained as a pale-yellow oil (2.72 g, 8.23 mmol, 40% yield).

^{1}H NMR (400 MHz, CDCl$_3$, 300 K) δ: 7.16 (dd, J = 5.2, 3.1 Hz, 1H), 6.74 (dd, J = 5.2, 1.5 Hz, 1H), 6.22 (dd, J = 3.1, 1.5 Hz, 1H), 3.96 (t, J = 6.3 Hz, 2H), 3.48 – 3.38 (m, 10 H), 3.33 (s, 3H), 1.90 – 1.80 (m, 2H), 1.77 – 1.70 (m, 2H), 1.68 – 1.61 (m, 8H).

^{13}C{^{1}H} NMR (101 MHz, CDCl$_3$, 300 K) δ: 158.0, 124.6, 119.5, 97.0, 72.6, 70.7, 70.6, 70.6, 70.4, 69.9, 58.5, 26.5, 26.4, 26.4, 26.3, 26.2.

HRMS (ESI): m/z calculated for $C_{17}H_{30}O_4S$: 330.1865, [M+H]$^+$ found: 331.1939.

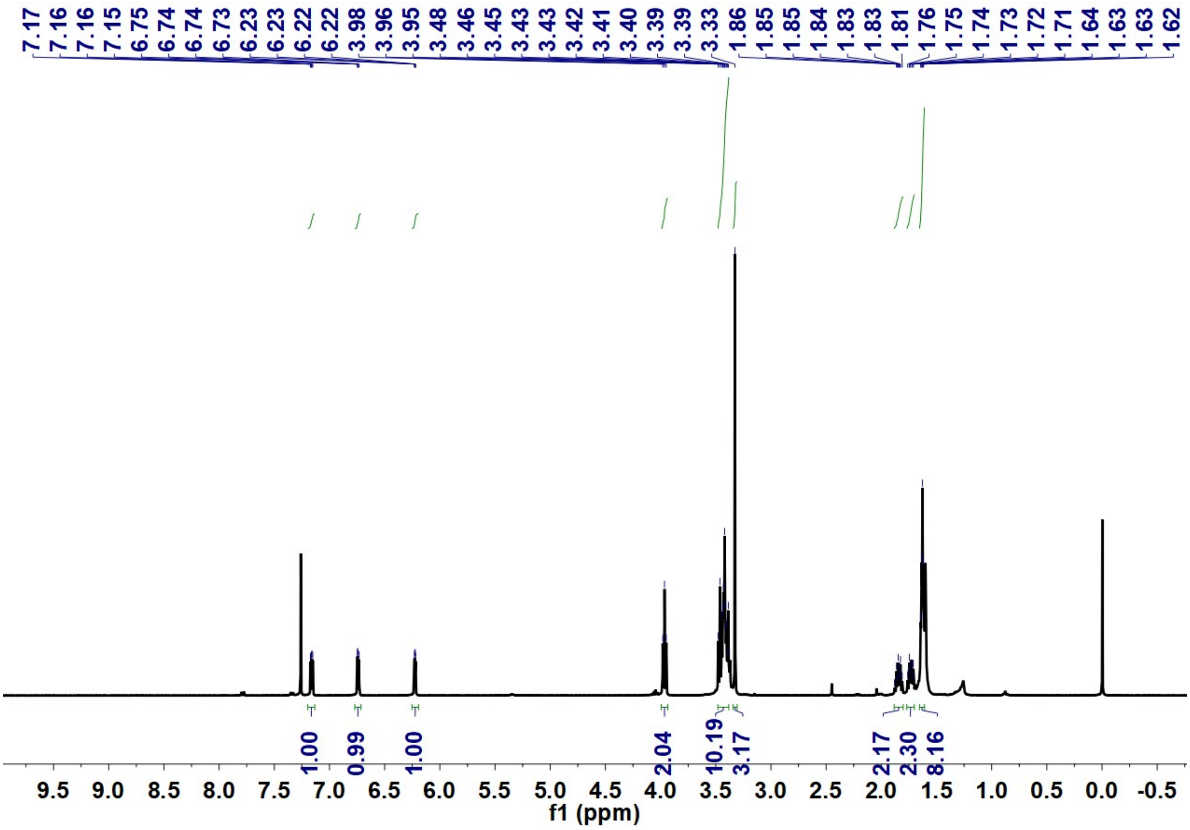

Fig S7 ^{1}H NMR spectrum of **S7c**.

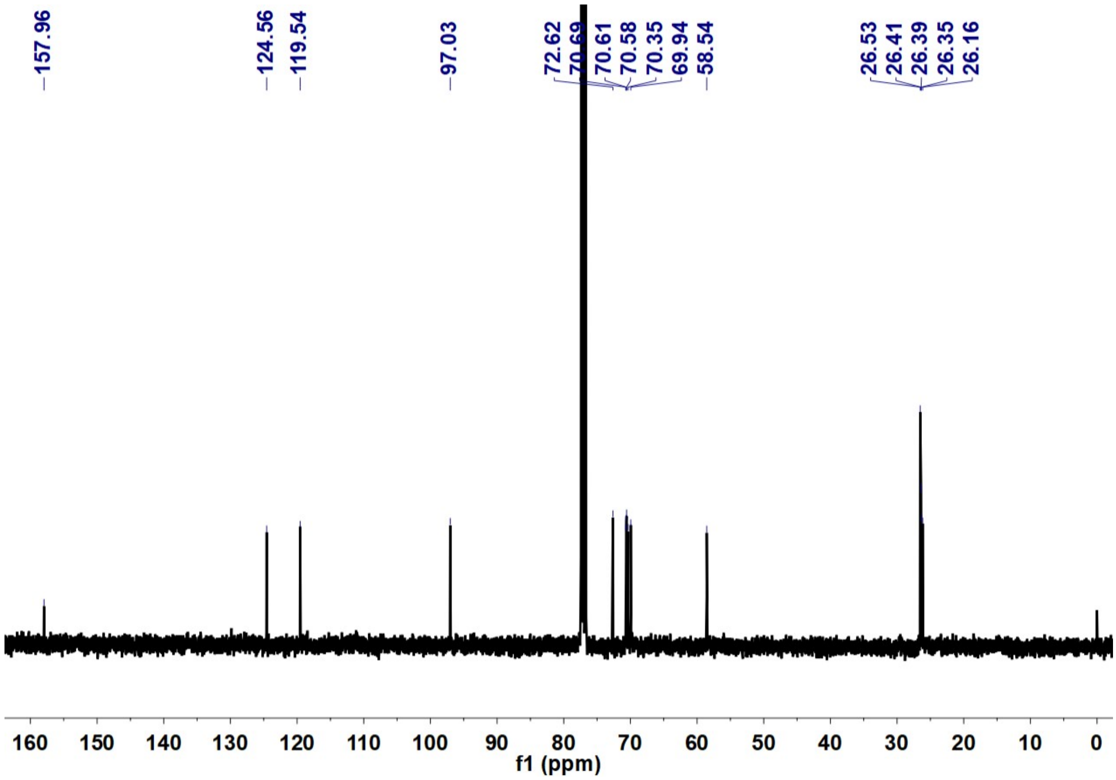

Fig S8 $^{13}C\{^1H\}$ NMR spectrum of **S7c**.

Synthesis of S8a-c

S8a: **S7a** (5.00 g, 20.3 mmol, 1.00 equiv.) was dissolved in a 9:1 v/v mixture of THF:hexane (100 mL) and cooled to 0 °C. N-bromosuccinimide (3.61 g, 20.3 mmol, 1.00 equiv.) was added portion wise over 5 min in the dark. The reaction mixture was stirred for 2 h at 0 °C. Distilled water was added to the reaction mixture and extracted with dichloromethane. The combined organic layers were washed with water and brine before being dried over anhydrous sodium sulfate. The crude product was purified by silica flash column chromatography to give the pure product as a yellow oil (6.27 g, 19.3 mmol, 95% yield).

S8b and **S8c** were synthesised analogously to **S8a**.

S8b: **S8b** was obtained as a pale-yellow oil (2.66 g, 7.24 mmol, 90% yield).

^1H NMR (400 MHz, $CDCl_3$, 300 K) δ: 7.19 (d, J = 5.9 Hz, 1H), 6.76 (d, J = 5.9 Hz, 1H), 4.14 (t, J = 6.2 Hz, 2H), 3.60 (t, J = 6.1 Hz, 2H), 3.54 – 3.42 (m, 8H), 3.33 (s, 3H), 2.04 – 1.98 (m, 2H), 1.87 – 1.80 (m, 4H).

$^{13}C\{^1H\}$ NMR (101 MHz, $CDCl_3$, 300 K) δ: 154.5, 124.2, 117.5, 91.7, 69.8, 69.1, 68.0, 67.8, 67.8, 67.0, 58.6, 30.0, 29.9, 29.6.

HRMS (ESI): *m/z* calculated for $C_{14}H_{23}BrO_4S$: 366.0500, $[M+H]^+$, found: 367.0573.

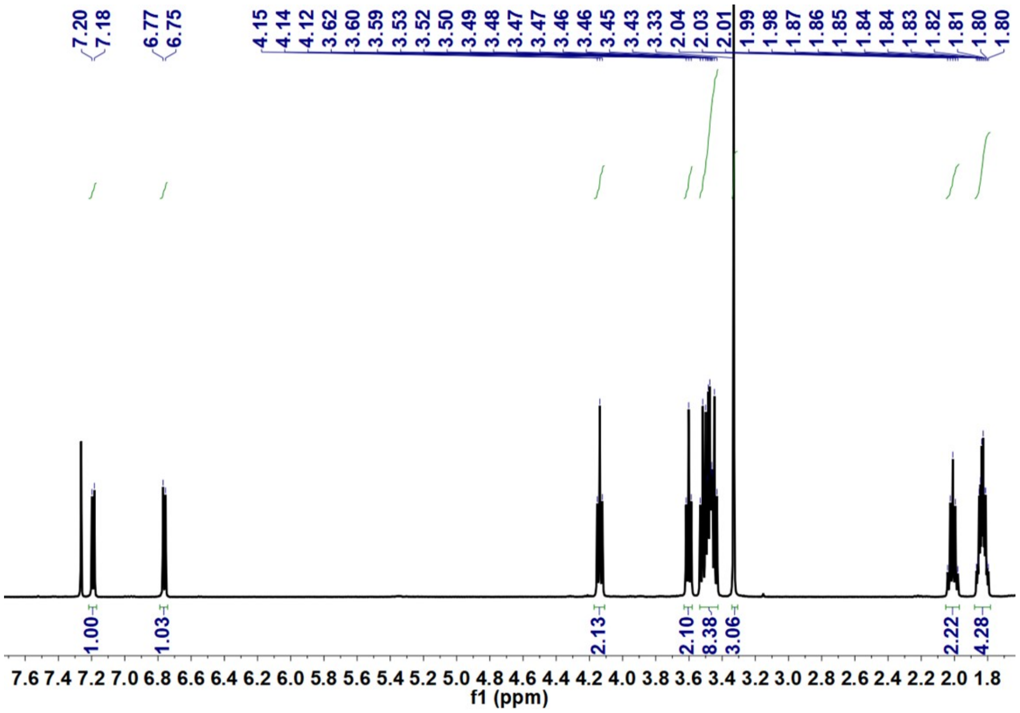

Fig S9 ^{1}H NMR spectrum of **S8b**.

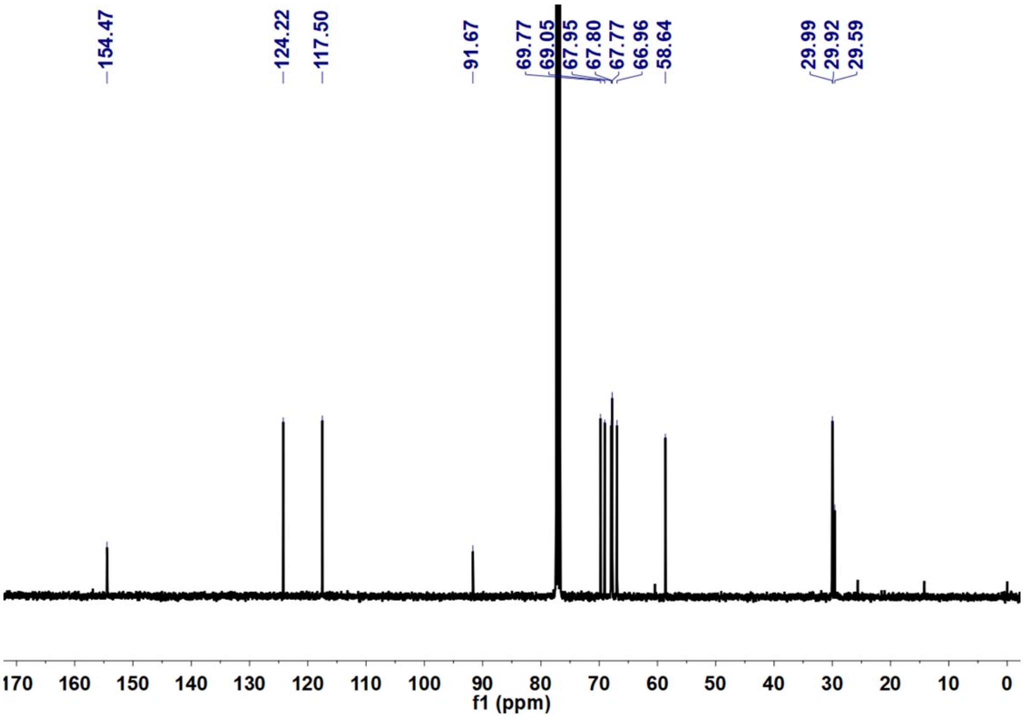

Fig S10 ^{13}C{^{1}H} NMR spectrum of **S8b**.

S8c: **S8c** was obtained as a pale-yellow oil (2.70 g, 6.58 mmol, 80% yield).

^{1}H NMR (400 MHz, CDCl$_3$, 300 K) δ: 7.19 (d, *J* = 5.9 Hz, 1H), 6.74 (d, *J* = 5.9 Hz, 1H), 4.06 (t, *J* = 6.0 Hz, 2H), 3.52 – 3.36 (m, 10H), 3.33 (s, 3H), 1.91 – 1.60 (m, 12H).

$^{13}C\{^{1}H\}$ NMR (101 MHz, $CDCl_3$, 300 K) δ: 154.5, 124.2, 117.5, 91.6, 72.6, 72.0, 70.7, 70.6, 70.6, 70.3, 58.5, 26.5, 26.4, 26.2.

HRMS (ESI): *m/z* calculated for $C_{17}H_{29}BrO_4S$: 408.0970, $[M+H]^+$, found: 409.1042.

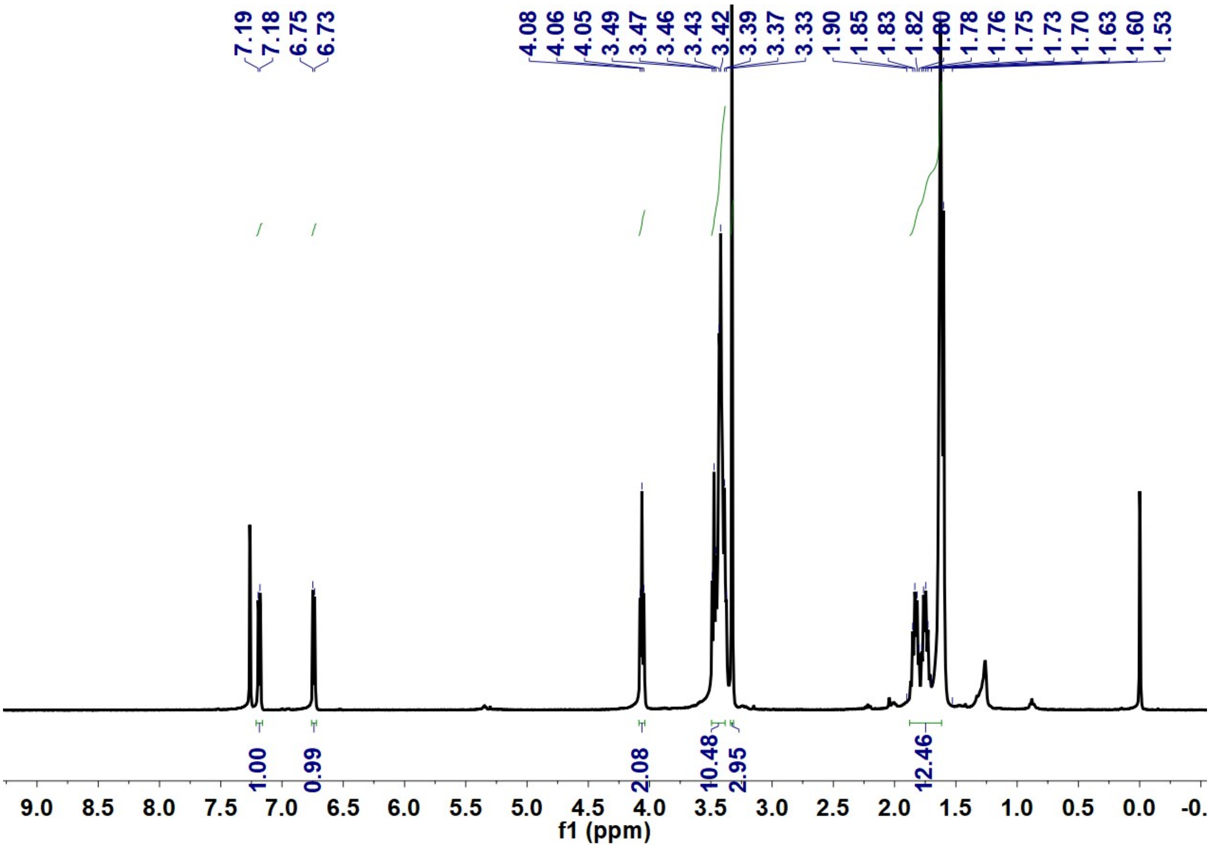

Fig S11 ^{1}H NMR spectrum of **S8c**.

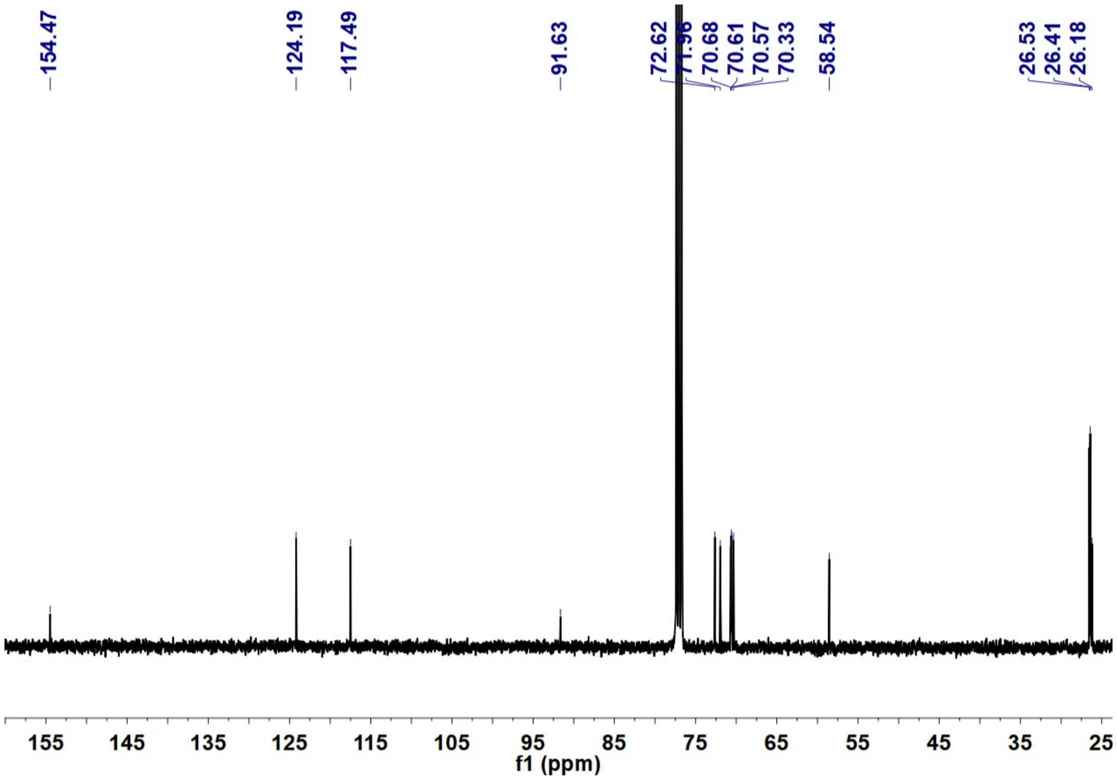

Fig S12 $^{13}C\{^{1}H\}$ NMR spectrum of **S8c**.

Synthesis of S9a-c

S9a: **S8a** (5.00 g, 15.4 mmol, 1.00 equiv.), 1,5-cyclooctadiene (1.60 g, 14.8 mmol, 0.961 equiv.) and 2,2'-bipyridine (2.85 g, 18.3 mmol, 1.19 equiv.) were dissolved in anhydrous THF (50 mL). Bis(1,5-cyclooctadiene) nickel (0) (4.05 g, 14.5 mmol, 0.942 equiv.) was added in one portion to the reaction mixture, leading to the formation of a dark purple solution. The resulting solution was heated to 66 °C overnight. Upon cooling to room temperature, the reaction mixture was filtered, and excess solvent was removed under reduced pressure. The crude product was purified by silica flash column chromatography to give the pure product as a pale-yellow solid (2.83 g, 5.78 mmol, 75% yield).

S9b and **S9c** were synthesised analogously to **S9a**.

S9b: **S9b** was obtained as a pale-yellow oil (1.77 g, 3.08 mmol, 85% yield).

^{1}H NMR (400 MHz, CDCl$_3$, 300 K) δ: 7.07 (d, J = 5.6 Hz, 2H), 6.85 (d, J = 5.6 Hz, 2H), 4.20 (t, J = 6.1 Hz, 4H), 3.68 (t, J = 6.2 Hz, 4H), 3.59 – 3.36 (m, 16H), 3.32 (s, 6H), 2.13 – 2.06 (m, 4H), 1.89 – 1.77 (m, 8H).

^{13}C{^{1}H} NMR (101 MHz, CDCl$_3$, 300 K) δ: 151.8, 121.7, 116.0, 114.0, 69.8, 68.7, 68.0, 67.8, 67.8, 67.4, 58.6, 30.1, 30.1, 30.0.

HRMS (ESI): *m/z* calculated for C$_{28}$H$_{46}$O$_8$S$_2$: 574.2634, [M+H]$^+$, found: 575.2701.

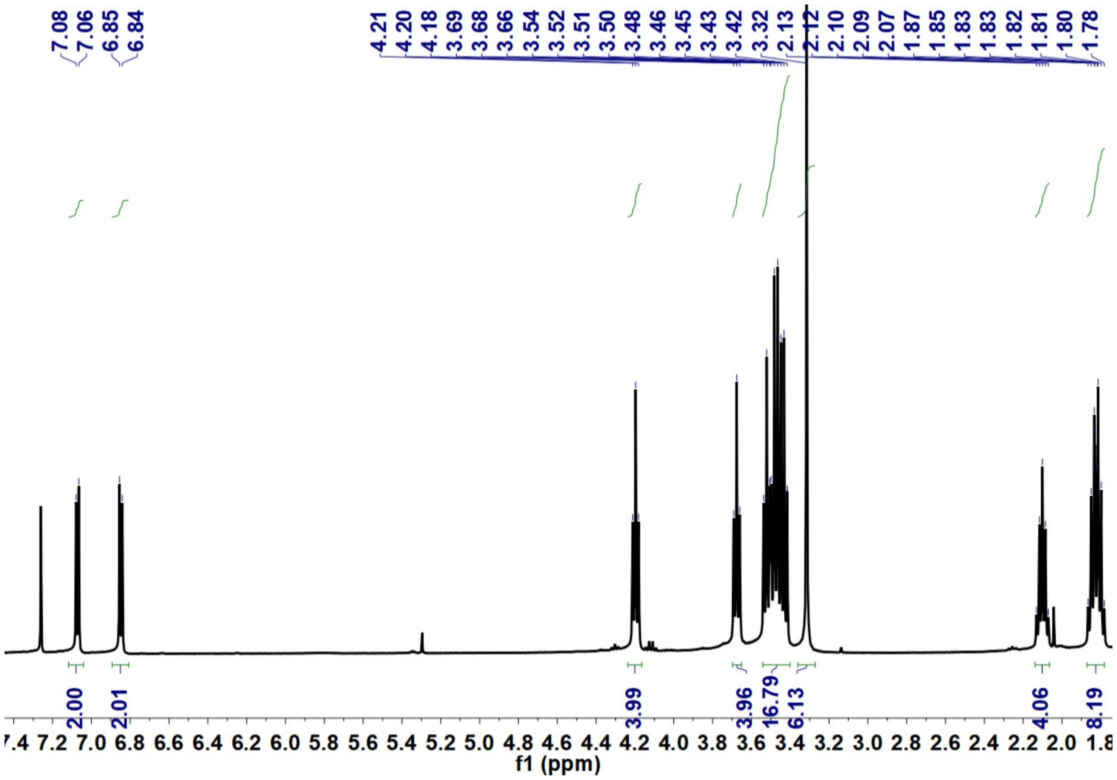

Fig S13 ^{1}H NMR spectrum of **S9b**.

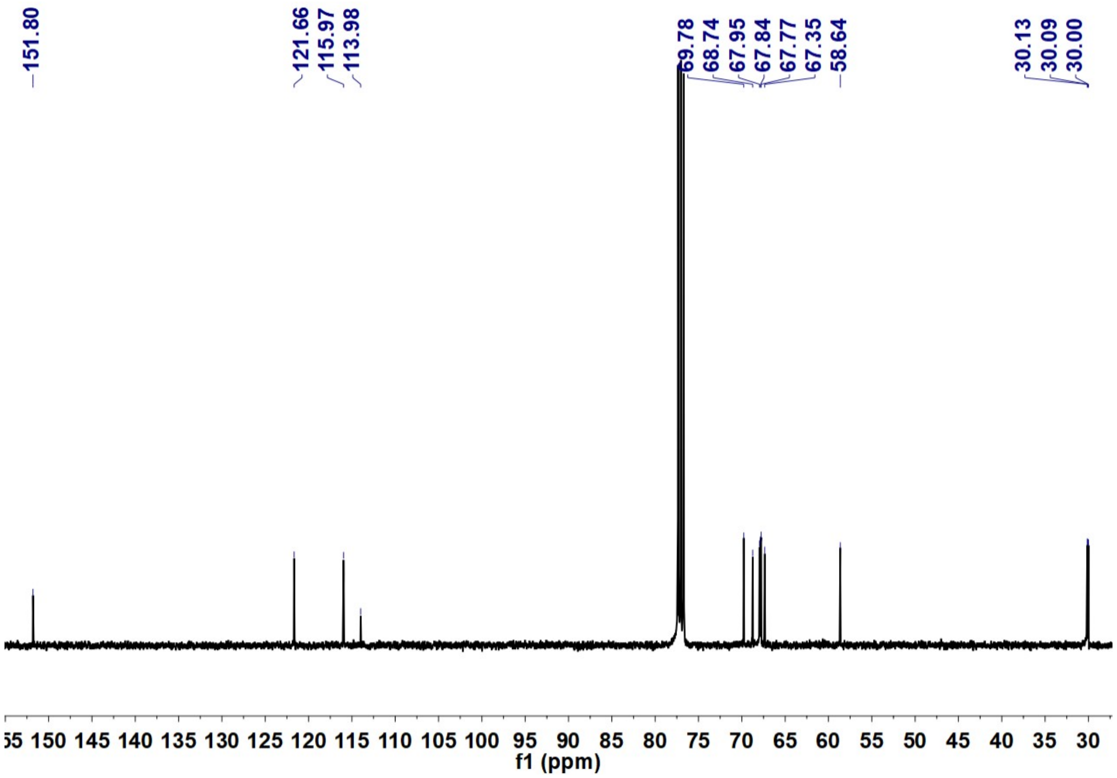

Fig S14 $^{13}C\{^1H\}$ NMR spectrum of **S9b**.

S9c: **S9c** was obtained as a pale-yellow oil (1.80 g, 2.80 mmol, 85% yield).

^1H NMR (400 MHz, $CDCl_3$, 300 K) *δ*: 7.07 (d, *J* = 5.6 Hz, 2H), 6.83 (d, *J* = 5.6 Hz, 2H), 4.12 (t, *J* = 6.2 Hz, 4H), 3.49 (t, *J* = 6.2 Hz, 4H), 3.52 – 3.36 (m, 16H), 3.32 (s, 6H), 1.99 – 1.87 (m, 4H), 1.87 – 1.77 (m, 4H), 1.67 – 1.58 (m, 16H).

$^{13}C\{^1H\}$ NMR (101 MHz, $CDCl_3$, 300 K) *δ*: 151.8, 121.7, 116.0, 114.1, 72.6, 71.7, 70.7, 70.6, 70.6, 70.4, 58.5, 26.6, 26.5, 26.4, 26.4.

HRMS (ESI): *m/z* calculated for $C_{34}H_{58}O_8S_2$: 658.3573, $[M+H]^+$, found: 659.3640.

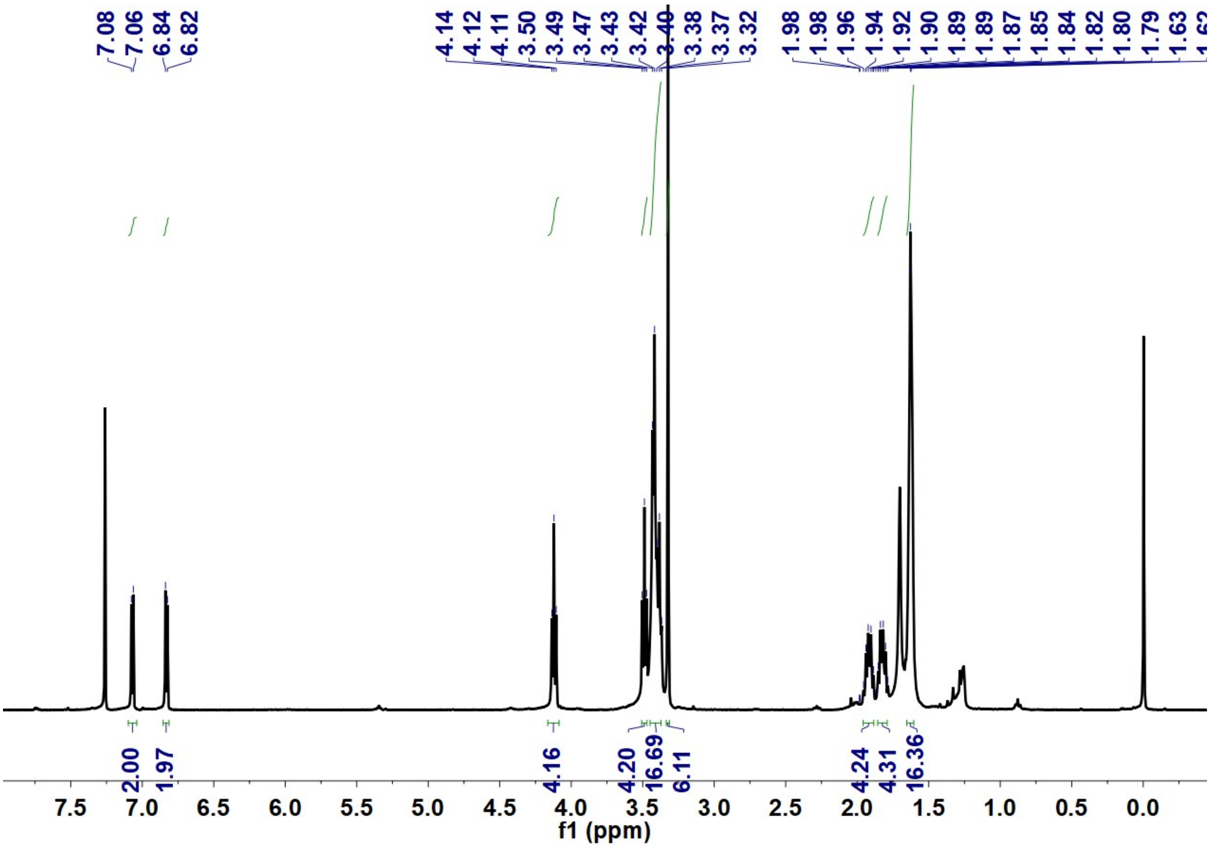

Fig S15 ^{1}H NMR spectrum of **S9c**.

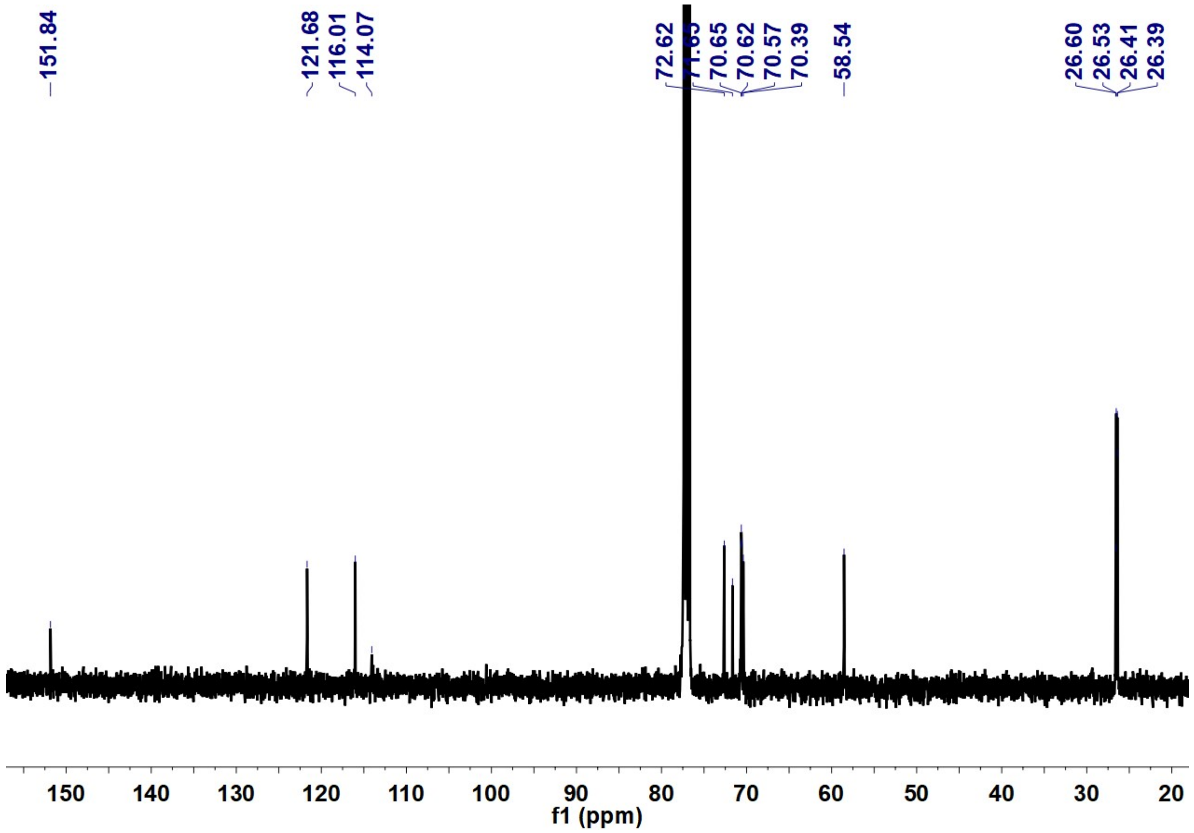

Fig S16 ^{13}C{^{1}H} NMR spectrum of **S9c**.

Synthesis of S10a-c

S10a: **S9a** (2.00 g, 4.08 mmol, 1.00 equiv.) was dissolved in anhydrous $CHCl_3$ (100 mL) and cooled to 0 °C. N-bromosuccinimide (1.45 g, 8.15 mmol, 2.00 equiv.) was added portion wise in the dark over 5 min. The reaction mixture was stirred at 0 °C for an additional 2 h. Water was poured into the reaction mixture and the aqueous layer extracted with dichloromethane. The combined organic layers were washed with water and brine before being dried over anhydrous sodium sulfate. The crude product was purified by silica flash column chromatography to give the pure product as an off-white solid **S10a** (2.22 g, 3.44 mmol, 84% yield).

S10b and **S10c** were synthesised analogously to **S10a**.

S10b: **S10b** was obtained as a pale-yellow oil (1.92 g, 2.62 mmol, 85% yield).

^1H NMR (400 MHz, $CDCl_3$, 300 K) δ: 6.84 (s, 2H), 4.15 (t, J = 6.2 Hz, 4H), 3.63 (t, J = 6.1 Hz, 4H), 3.55 – 3.40 (m, 16H), 3.32 (s, 6H), 2.14 – 2.02 (m, 4H), 1.91 – 1.78 (m, 8H).

$^{13}C\{^1H\}$ NMR (101 MHz, $CDCl_3$, 300 K) δ: 150.3, 119.1, 115.0, 109.9, 69.8, 69.2, 68.0, 67.8, 67.8, 67.0, 58.6, 30.1, 30.0.

HRMS (ESI): m/z calculated for $C_{28}H_{44}Br_2O_8S_2$: 732.0824, $[M+H]^+$, found: 733.0899.

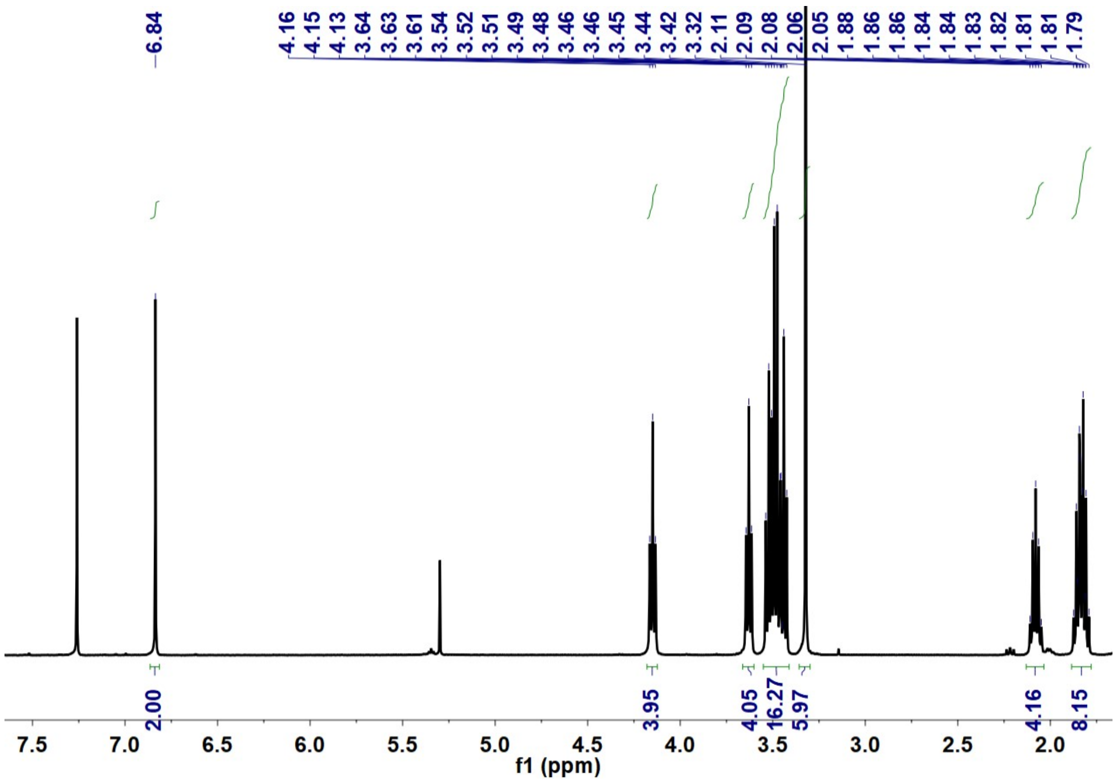

Fig S17 ^{1}H NMR spectrum of **S10b**.

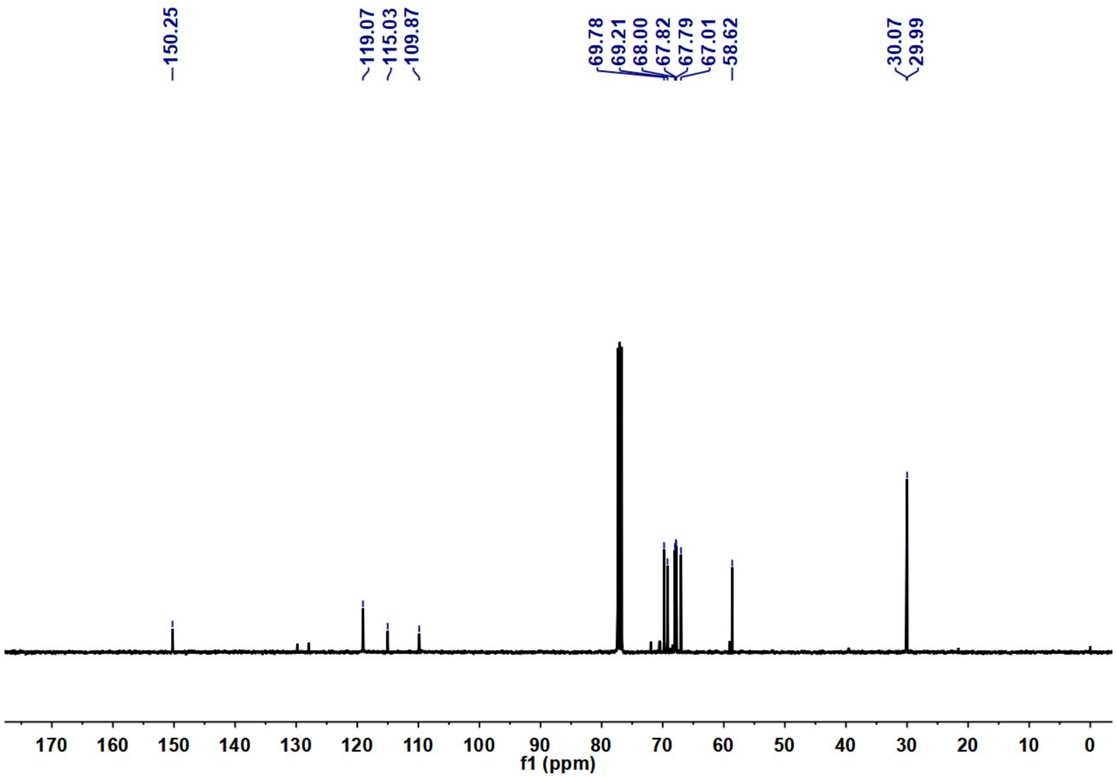

Fig S18 ^{13}C{^{1}H} NMR spectrum of **S10b**.

S10c: **S10c** was obtained as a pale-yellow oil (1.80 g, 2.24 mmol, 80% yield).

^{1}H NMR (400 MHz, CDCl$_3$, 300 K) δ: 6.81 (s, 2H), 4.07 (t, *J* = 6.4 Hz, 4H), 3.49 (t, *J* = 6.2 Hz, 4H), 3.46 – 3.36 (m, 16H), 3.32 (s, 6H), 1.94 – 1.87 (m, 4H), 1.81 – 1.74 (m, 4H), 1.68 – 1.58 (m, 16H).

^{13}C{^{1}H} NMR (101 MHz, CDCl$_3$, 300 K) δ: 150.3, 119.1, 115.1, 109.9, 72.6, 72.1, 70.7, 70.6, 70.6, 70.2, 58.5, 26.5, 26.5, 26.4, 26.4, 26.2.

HRMS (ESI): *m/z* calculated for $C_{34}H_{56}Br_2O_8S_2$: 816.1763, [M+H]$^+$, found: 817.1830.

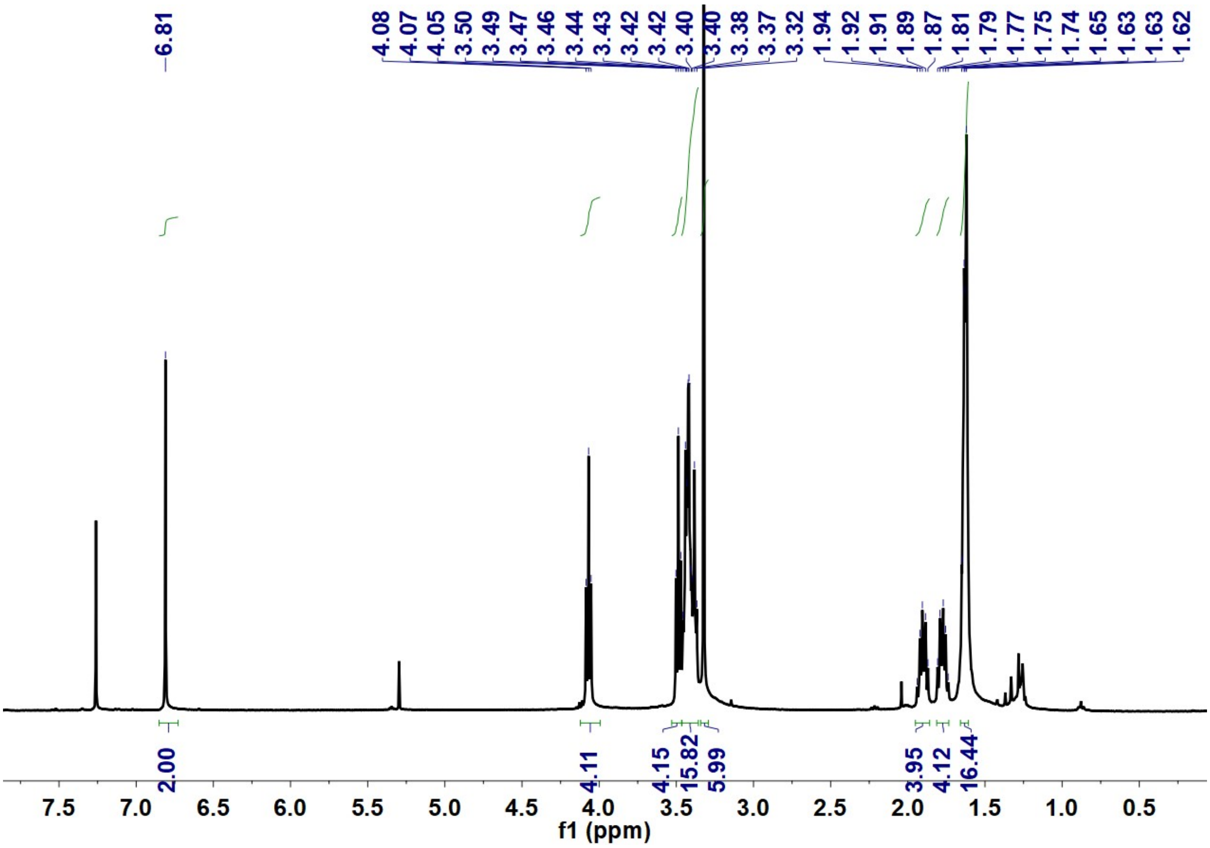

Fig S19 ^{1}H NMR spectrum of **S10c**.

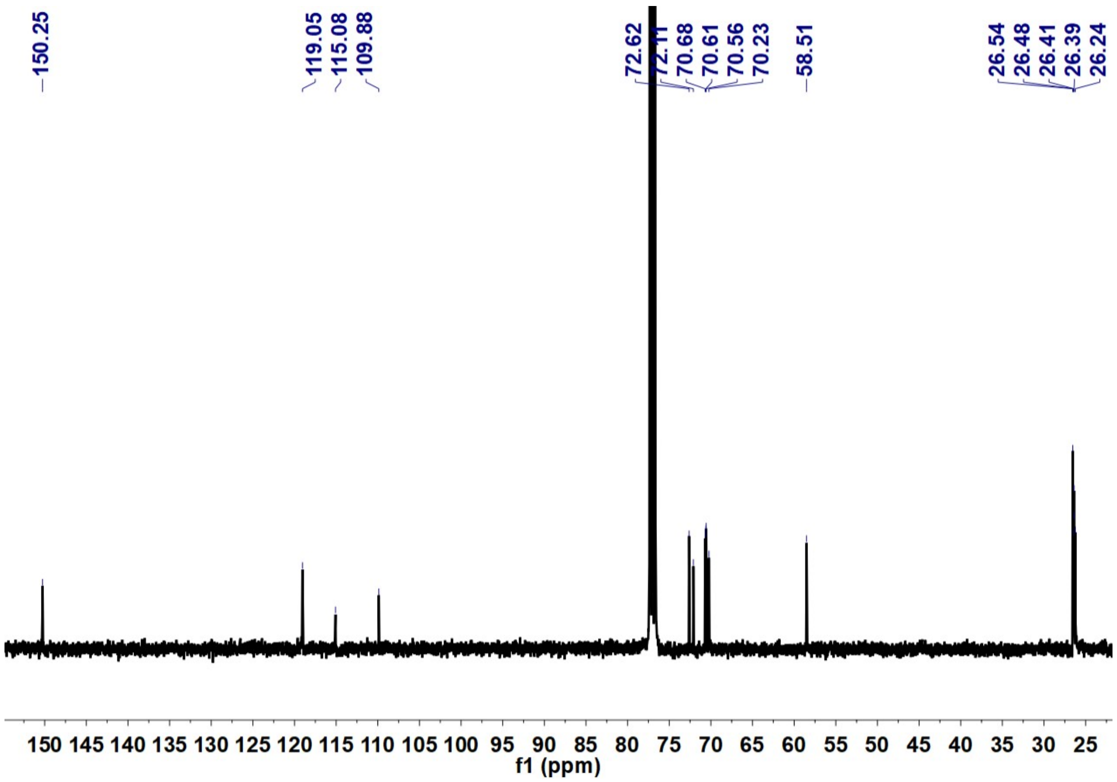

Fig S20 $^{13}C\{^{1}H\}$ NMR spectrum of **S10c**.

2.3 Polymer Synthesis

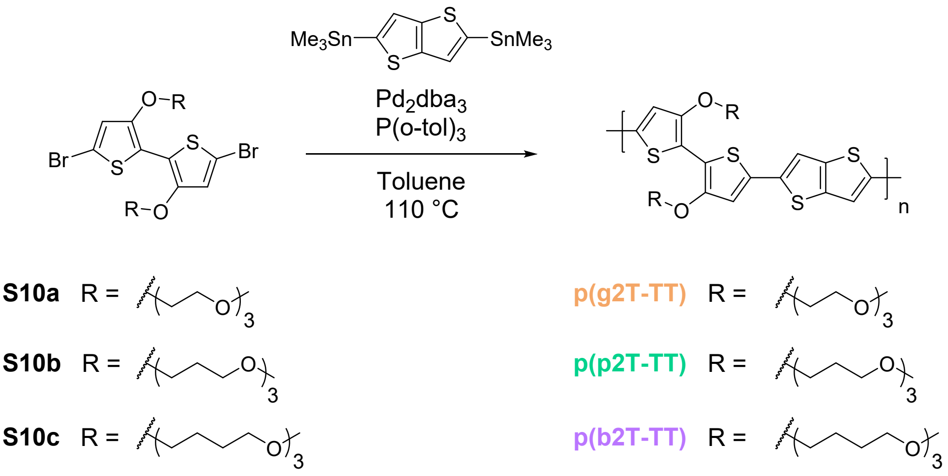

Scheme S3 Synthesis of **p(g2T-TT)**, **p(p2T-TT)**, and **p(b2T-TT)**.

p(g2T-TT): S10a (100.0 mg, 0.1548 mmol, 1.000 equiv.), 2,5-bis(trimethylstannyl)thieno[3,2-b]thiophene (71.84 mg, 0.1542 mmol, 0.9963 equiv.), $Pd_2(dba)_3$ (2.00 mg, $2.19 \cdot 10^{-3}$ mmol, 0.0141 equiv.) and $P(o\text{-}tol)_3$ (4.00 mg, 0.0131 mmol, 0.0849 equiv.) were added to a microwave vial. The tube was sealed and flushed with argon. Anhydrous and degassed toluene (1 mL) was added, and the mixture further degassed. The reaction was then heated to 110 °C for 24 h. After cooling to RT, the polymer was precipitated into methanol, and filtered through a Soxhlet thimble. The crude polymer was purified by Soxhlet extractions with methanol, acetone, hexane, and dichloromethane. The product was collected in dichloromethane and the dichloromethane fraction was concentrated under reduced pressure. The final polymer was obtained by precipitation into methanol and the solid was collected by suction filtration. Ultimately, **p(g2T-TT)** was collected as a dark blue solid (82 mg, 85% yield).

^1H NMR (500 MHz, 1,1,2,2-tetrachloroethane-d_2, 393 K) δ: 7.60 – 6.79 (broad), 4.86 – 4.26 (broad), 4.25 – 3.02 (m).

GPC ($CHCl_3$, 40 °C): M_n = 24.7 kDa, $Đ$ = 1.4. Note: as previously observed for EG functionalised conjugated polymers, a bimodal elution profile for the polymer was recorded.[6,7] As the shorter elution time (higher molecular weight) peak has previously been attributed to polymer aggregation, to forego molecular weight overestimation, the signal for this peak was neglected.

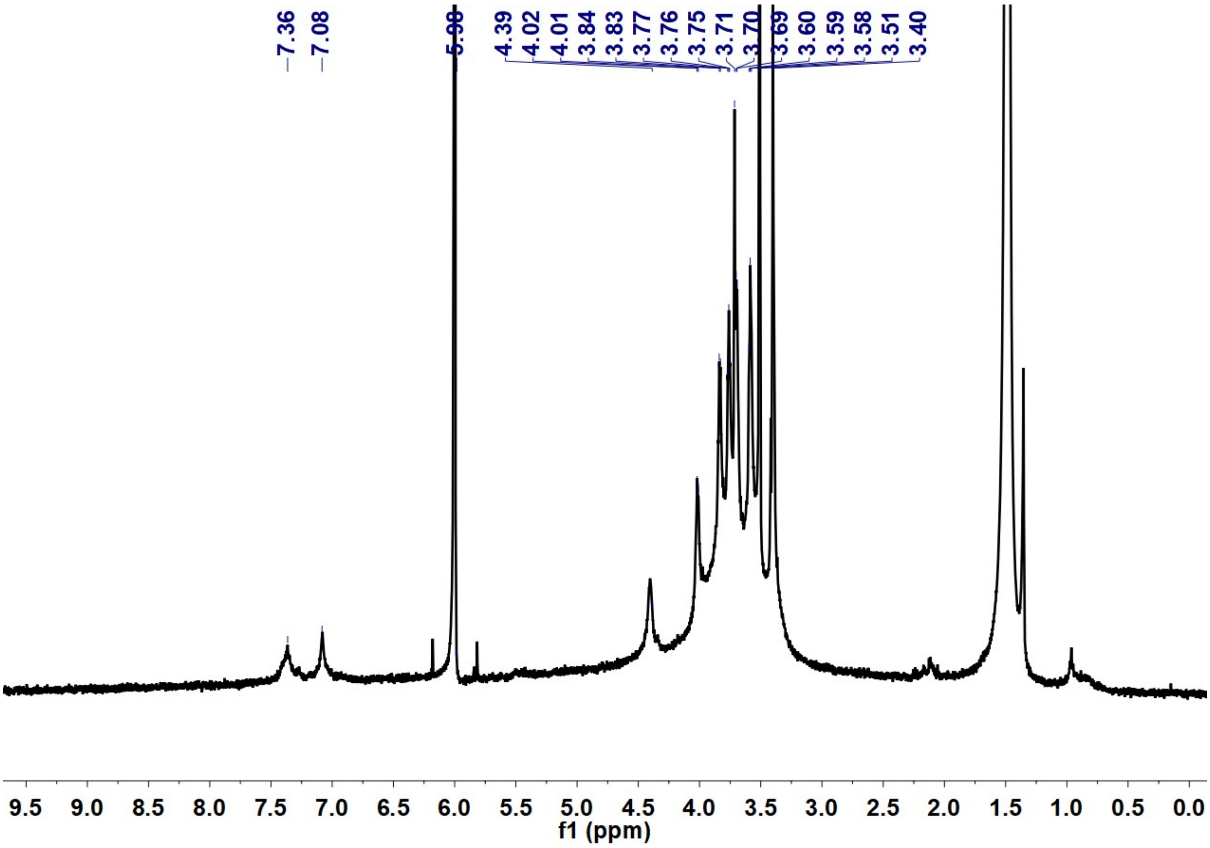

Fig S21 ^{1}H NMR spectrum of **p(g2T-TT)**.

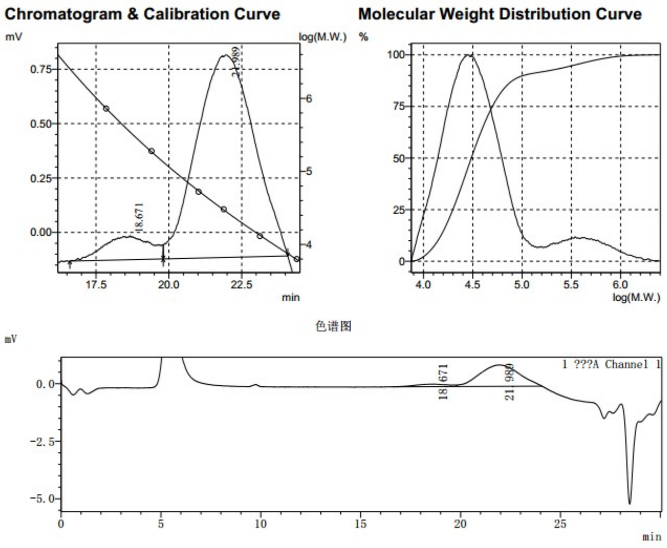

Fig S22 GPC data recorded for **p(g2T-TT)**.

p(p2T-TT) and **p(b2T-TT)** were synthesised analogously to **p(g2T-TT)**.

p(p2T-TT): Dark blue solid (87 mg, 89% yield).

^{1}H NMR (500 MHz, 1,1,2,2-tetrachloroethane-d_2, 393 K) δ: 7.54 – 7.10 (broad), 7.10 – 6.15 (broad), 4.70 – 3.99 (broad), 3.96 – 2.88 (m), 2.40 – 1.70 (m).

GPC (CHCl$_3$, 40 °C): M_n = 24.7 kDa, $Đ$ = 1.4. Note: as previously observed for EG functionalised conjugated polymers, a bimodal elution profile for the polymer was recorded.[6,7] As the shorter elution time (higher molecular weight) peak has previously been attributed to polymer aggregation, to forego molecular weight overestimation, the signal for this peak was neglected.

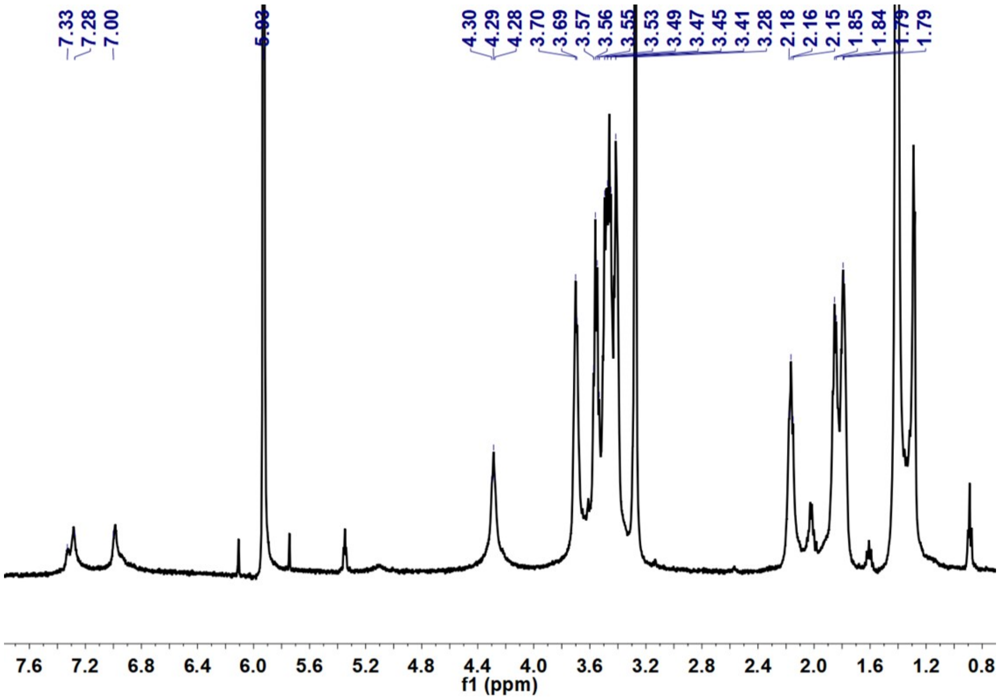

Fig S23 ^{1}H NMR spectrum of **p(p2T-TT)**.

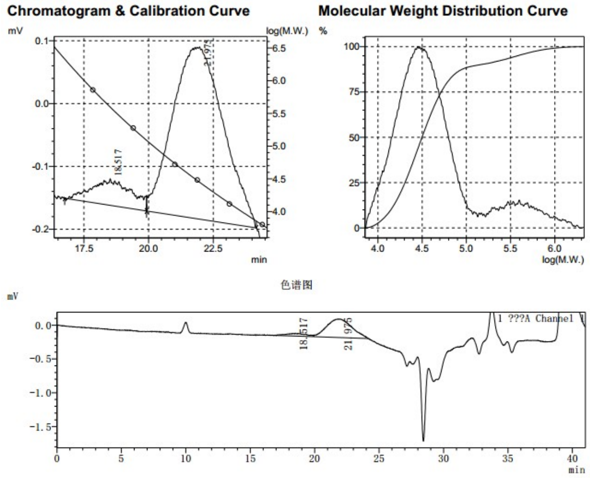

Fig S24 GPC data recorded for **p(p2T-TT)**.

p(b2T-TT): Dark blue solid (86 mg, 88% yield).

^{1}H NMR (500 MHz, 1,1,2,2-tetrachloroethane-d_2, 393 K) δ: 7.44 – 7.11 (broad), 7.10 – 6.70 (broad), 4.49 – 4.10 (broad), 3.97 – 3.12 (m), 2.20 – 2.12 (m), 2.07 – 1.90 (m), 1.90 – 1.78 (m), 1.73 – 1.51 (m).

GPC ($CHCl_3$, 40 °C): M_n = 19.8 kDa, $Đ$ = 1.5. Note: as previously observed for EG functionalised conjugated polymers, a bimodal elution profile for the polymer was recorded.[6,7] As the shorter elution time (higher molecular weight) peak has previously been attributed to polymer aggregation, to forego molecular weight overestimation, the signal for this peak was neglected.

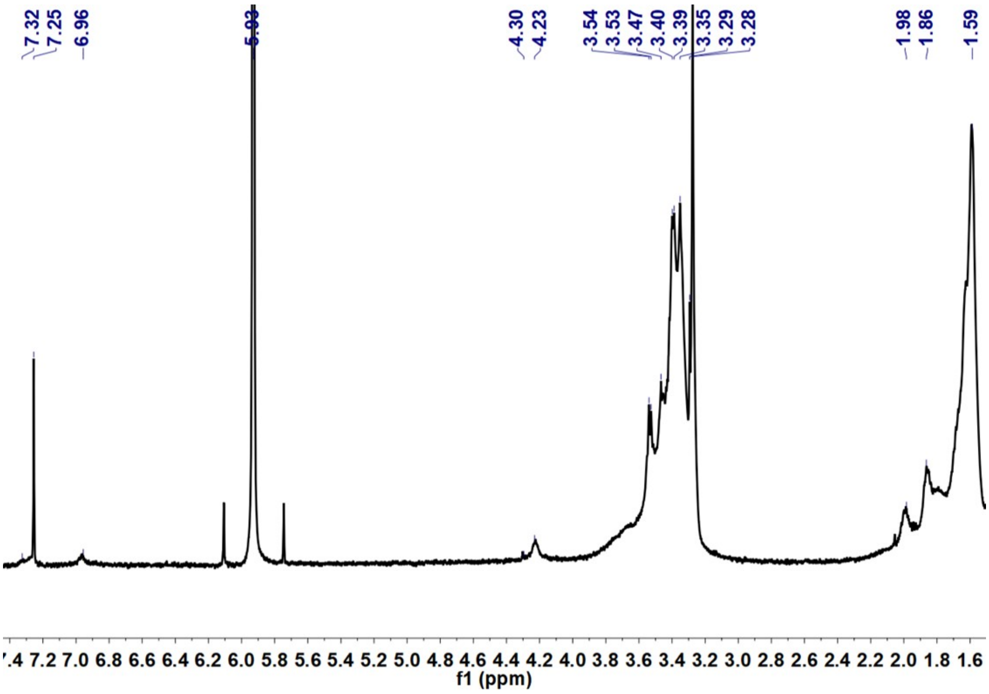

Fig S25 ^{1}H NMR spectrum of **p(b2T-TT)**.

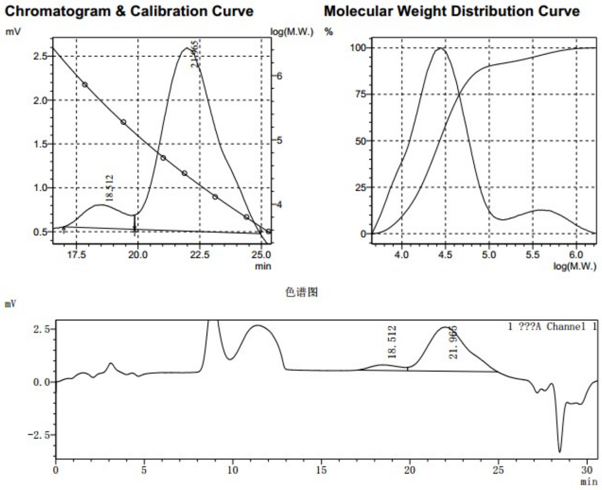

Fig S26 GPC data recorded for **p(b2T-TT)**.

3. UV-Vis Absorption Spectroscopy

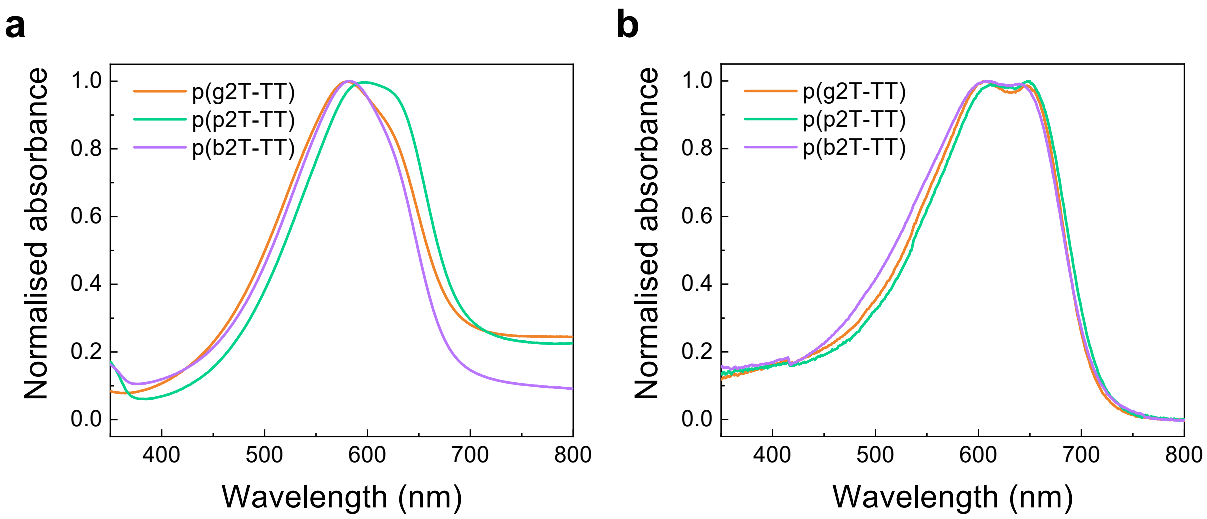

Fig S27 Normalised UV-Vis absorption spectra of the polymers in a) dilute chloroform solution at room temperature and b) thin film while applying a negative potential to ensure complete dedoping of the polymer films.

4. Cyclic Voltammetry

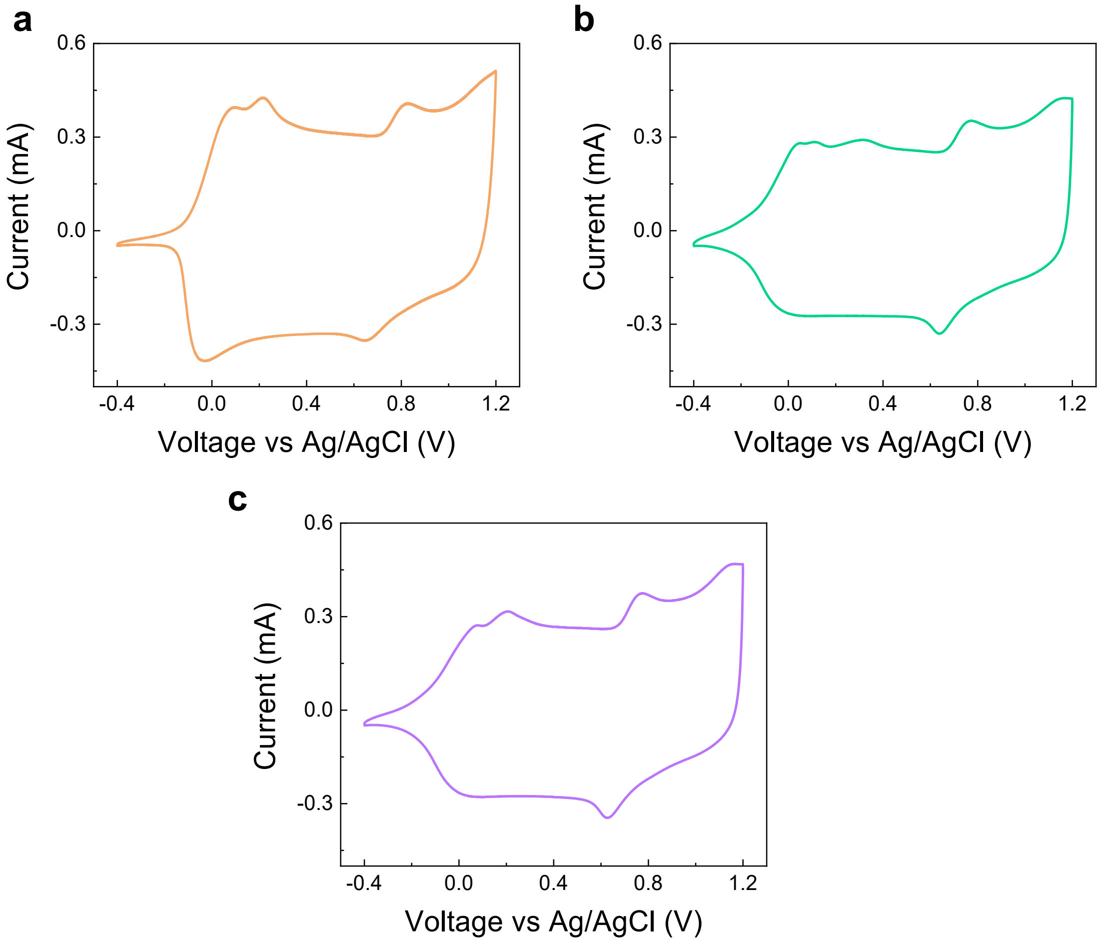

Fig S28 Cyclic voltammograms recorded for (a) p(g2T-TT), (b) p(p2T-TT), and (c) p(b2T-TT) employing a 0.1 M tetrabutylammonium hexafluorophosphate solution in acetonitrile as the supporting electrolyte.

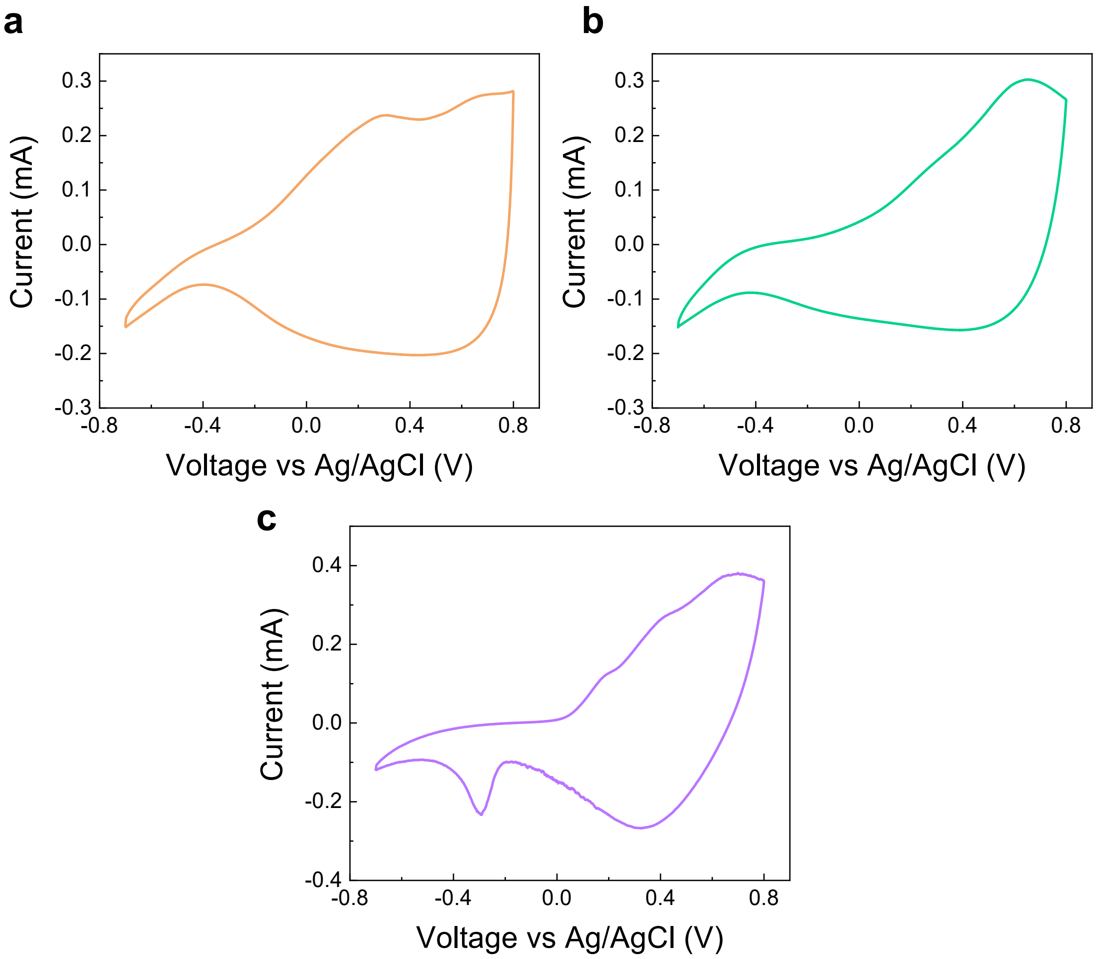

Fig S29 Cyclic voltammograms recorded for (a) p(g2T-TT), (b) p(p2T-TT), and (c) p(b2T-TT) employing an aqueous 0.1 M sodium chloride solution as the supporting electrolyte.

5. Spectroelectrochemistry

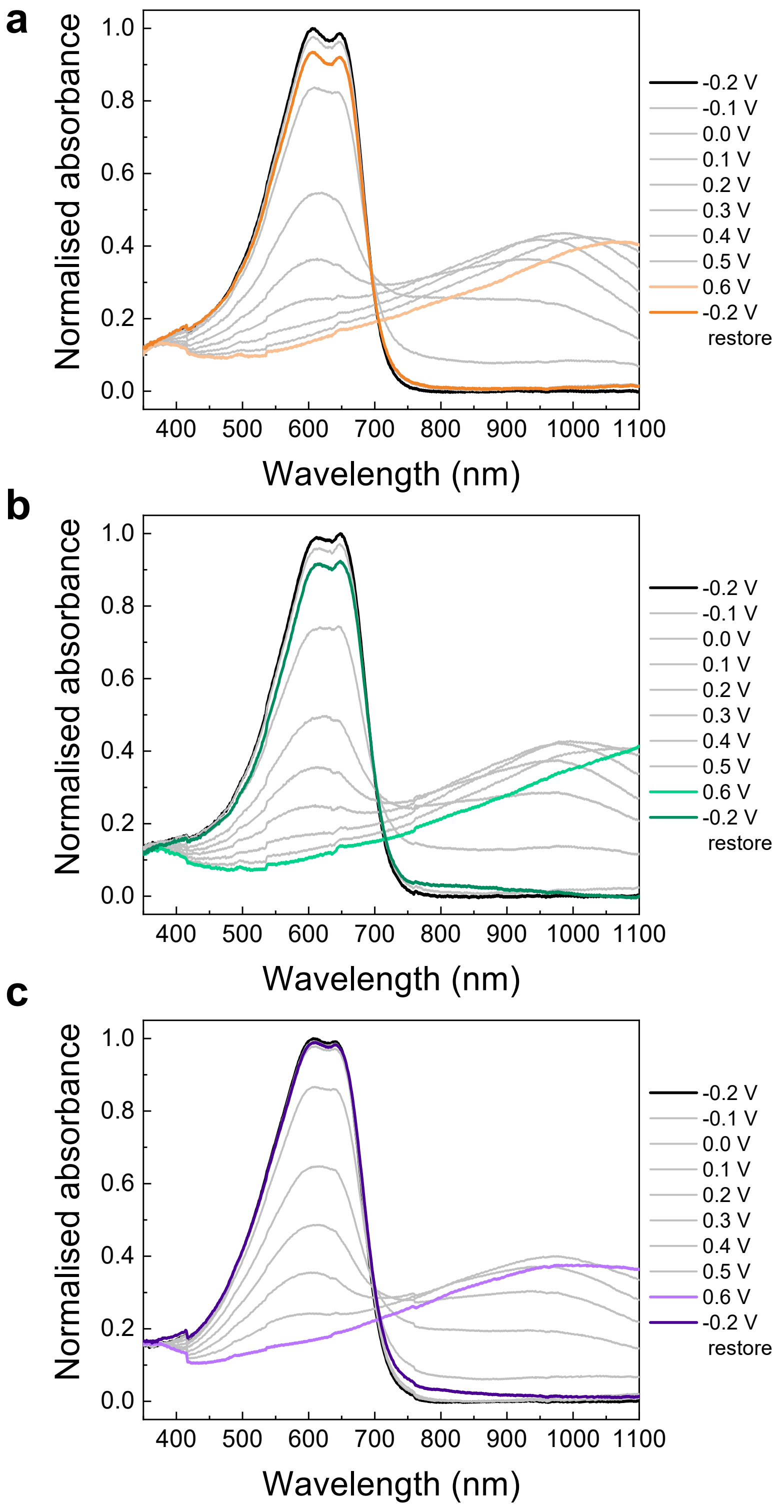

Fig S30 Spectroelectrochemical measurements conducted for (a) p(g2T-TT), (b) p(p2T-TT), and (c) p(b2T-TT) employing an aqueous 0.1 M sodium chloride solution as the supporting electrolyte.

6. Organic Electrochemical Transistors

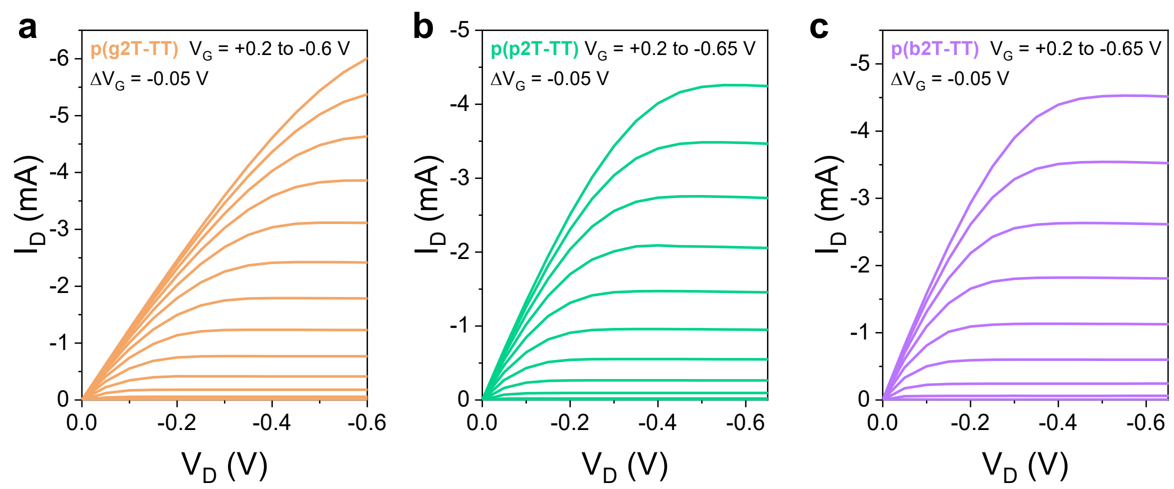

Fig S31 OECT output curves for (a) p(g2T-TT), (b) p(p2T-TT), and (c) p(b2T-TT).

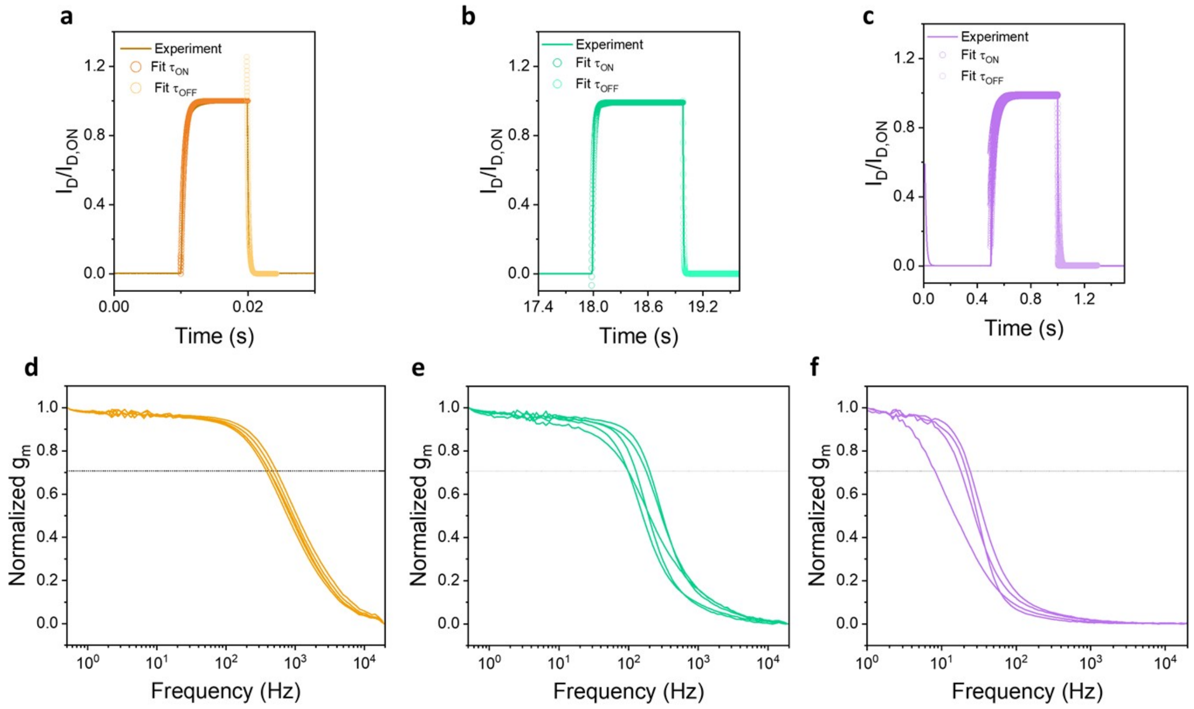

Fig S32 Transient profiles of (a) p(g2T-TT), (b) p(p2T-TT), and (c) p(p2T-TT), and bandwidth curves of (d) p(g2T-TT), (e) p(p2T-TT), and (f) p(p2T-TT) for the estimation of the OECTs' on (τ_{on}) and off (τ_{on}) switching speeds. The dotted lines in the bandwidth profiles represent the

-3 dB level, where the cut-off frequency was extracted. Thickness values for (a,d) are 80.1 ± 2.9 nm, for (b,e) 134.8 ± 18.6 nm, and for (c,f) 137.7 ± 8.2 nm.

Table S1. Summary of the response time characteristics of OECTs

Polymer	**τ_{ON}[a]**	**τ_{OFF}[b]**	**$f_{cut\text{-}off}$ τ_{ON}**	**d (nm)**
p(g2T-TT)	456.57 ± 5.2 μs	139.55 ± 8.1 μs	360.82 ± 36.1 μs	80.1 ± 2.9
p(p2T-TT)	1.11 ± 0.11 ms	0.25 ± 0.015 ms	1.24 ± 0.31 ms	134.8 ± 18.6
p(b2T-TT)	30.04 ± 3.08 ms	6.6 ± 3.67 ms	10.54 ± 4.42 ms	137.7 ± 8.2

[a] τ_{ON} estimated from a single exponential decay fit of the drain current response to a square shape V_G pulse (V_G increases from 0 to -0.6 V for p(p2T-TT) and p(b2T-TT), and from 0 to -0.5 V for p(g2T-TT)). The pulse length is 10 ms for p(g2T-TT), 1 sec for p(p2T-TT), and 500 ms for p(b2T-TT), and V_D = -0.6 V in all cases. [b] τ_{OFF} estimated from a single exponential decay fit of the I_D response going from the ON state back to V_G =0 V (OFF state). [c] τ_{ON} estimated from the cut-off frequency.

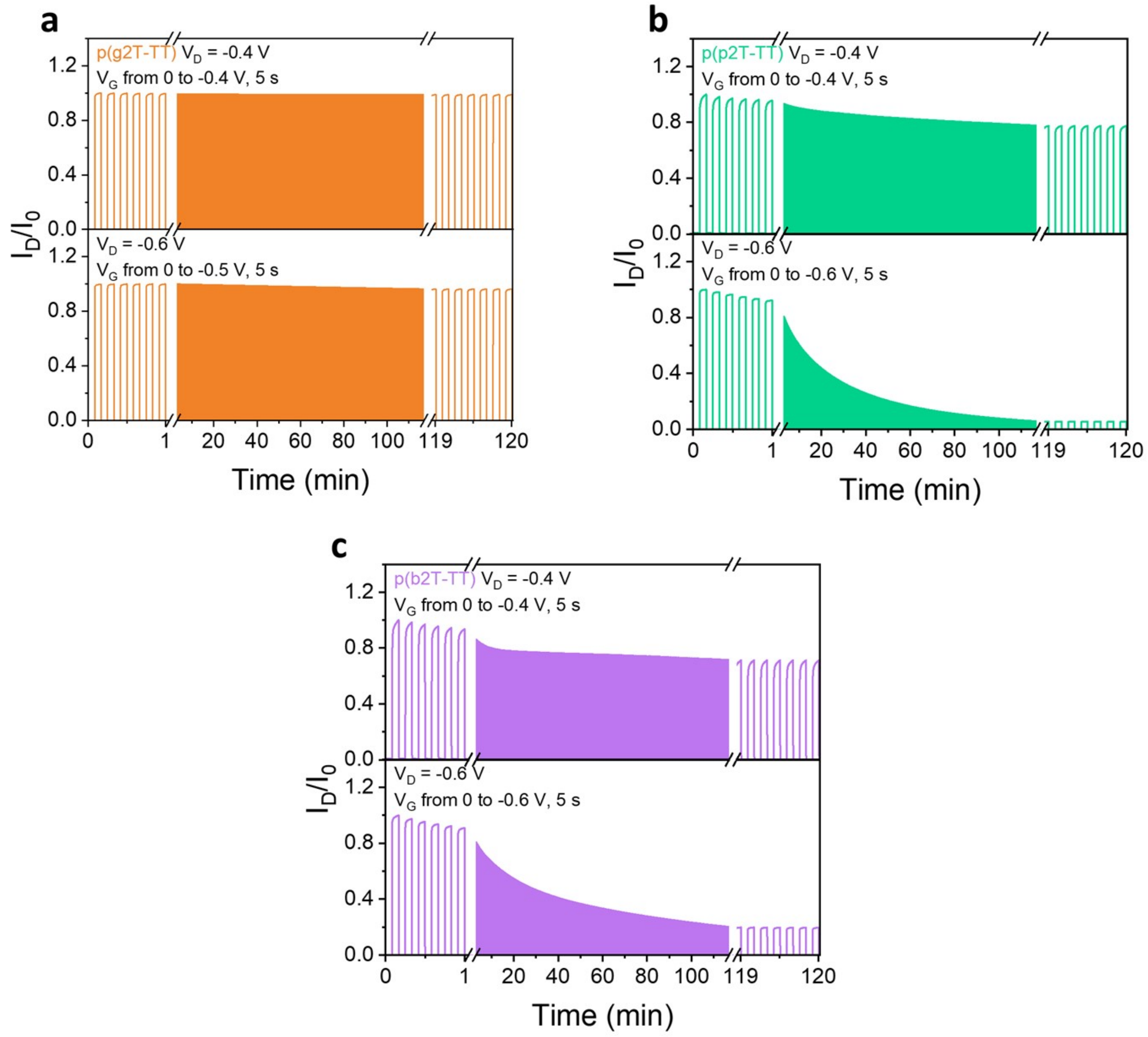

Fig S33 Voltage pulses (5 sec on, 5 sec off) applied at the gate electrode for 2 hours for OECTs made of a) p(g2T-TT), b) p(p2T-TT), and c) p(b2T-TT). The devices are in the saturation regime for the two drain voltages selected (-0.4 V, -0.6V) and the gate voltages applied are -0.4 V, -0.5 V or -0.6V.

7. AFM Images

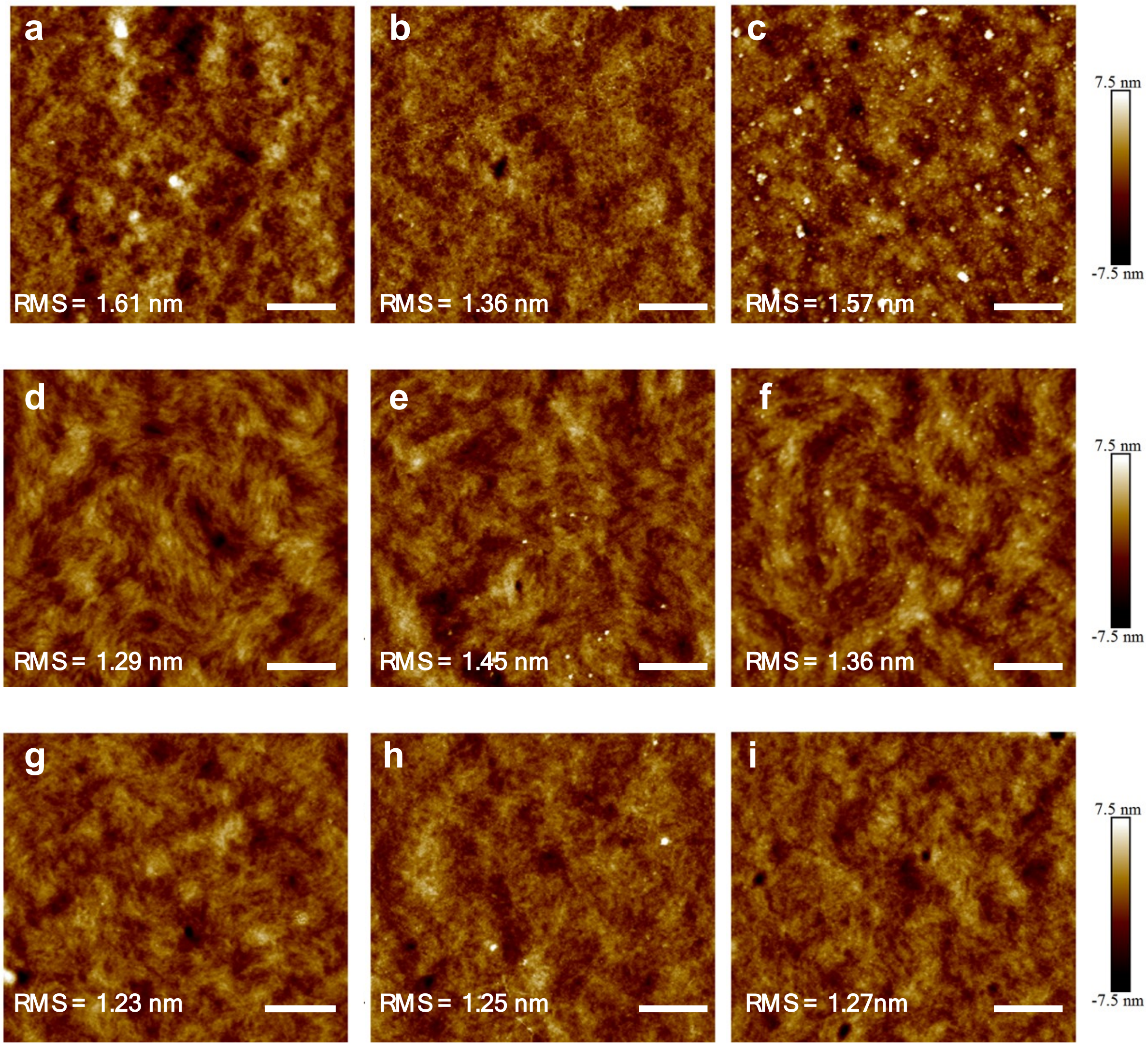

Fig S34 AFM height images taken for p(g2T-TT) – 1st row, p(p2T-TT) – 2nd row, and p(b2T-TT) – 3rd row. (a,d,g) Images taken for the pristine polymer samples. (b,e,h) Images taken for hydrated polymer samples. (c,f,i) Images taken for the electrochemically doped polymer samples. For each image the scale bar is 400 nm.

8. Electrochemical Impedance Spectroscopy

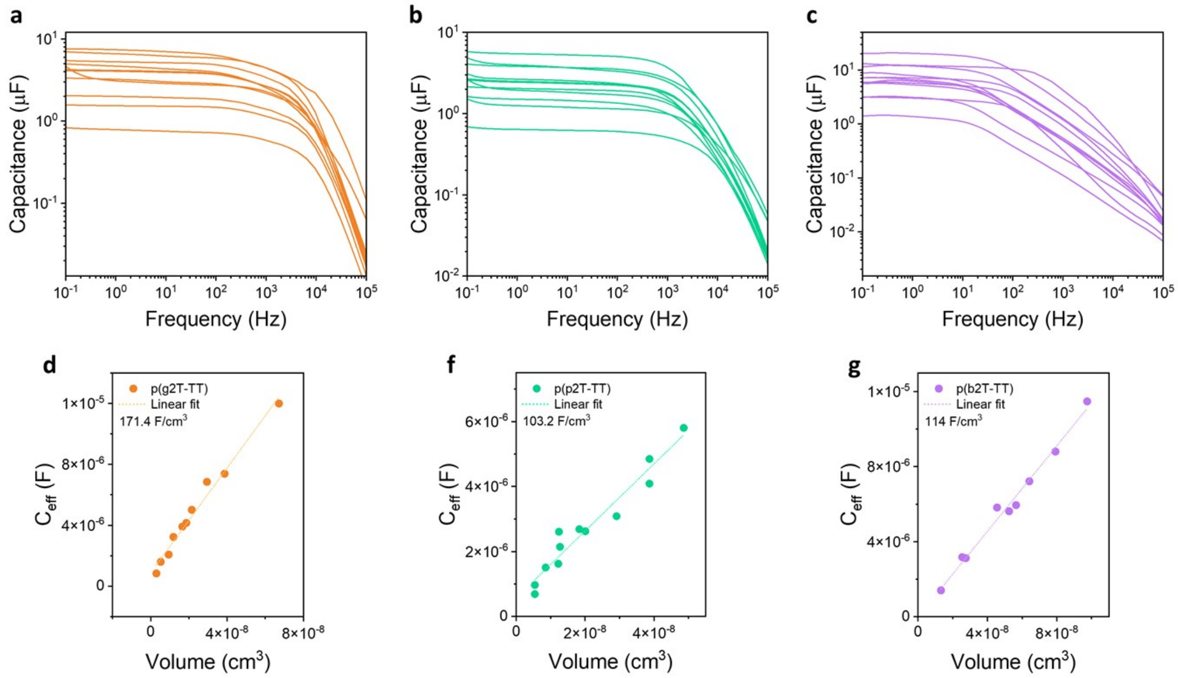

Fig S35 Effective capacitance curves vs frequency recorded for a variety of electrode sizes with (a) p(g2T-TT), (b) p(p2T-TT), and (c) p(b2T-TT). For each polymer, electrochemical impedance spectra were recorded by applying an offset voltage which corresponds to the gate voltage incurring the highest transistor performance. The capacitance values at 0.1 Hz were plotted as a function of film volume for (d) p(g2T-TT), (e) p(p2T-TT), and (f) p(b2T-TT), yielding the volumetric capacitance.

9. GIWAXS Measurements

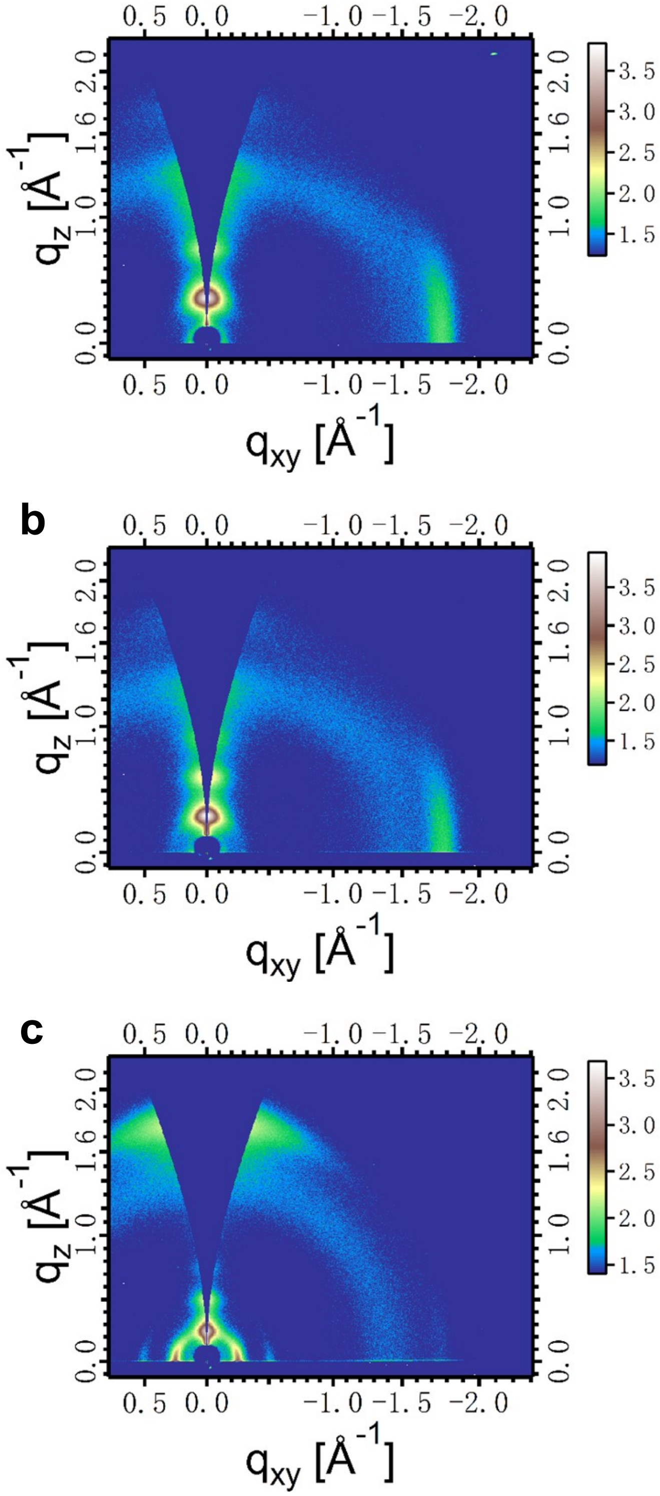

Fig S36 GIWAXS patterns recorded for (a) p(g2T-TT), (b) p(p2T-TT), and (c) p(b2T-TT).

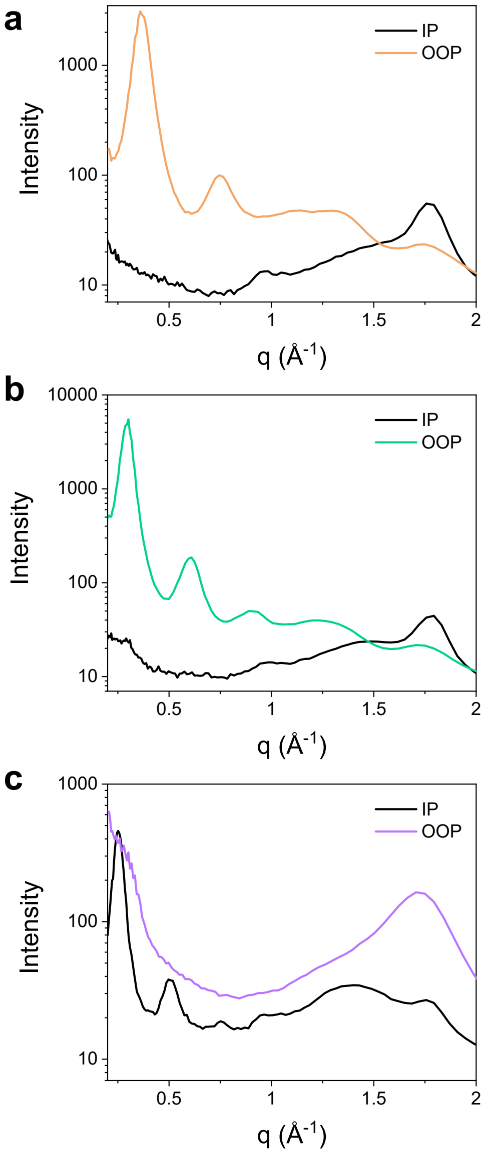

Fig S37 In-plane and out-of-plane GIWAXS linecuts for spin-cast films of (a) p(g2T-TT), (b) p(p2T-TT), and (c) p(b2T-TT).

10. Electrochemical Quartz Crystal Microbalance with Dissipation

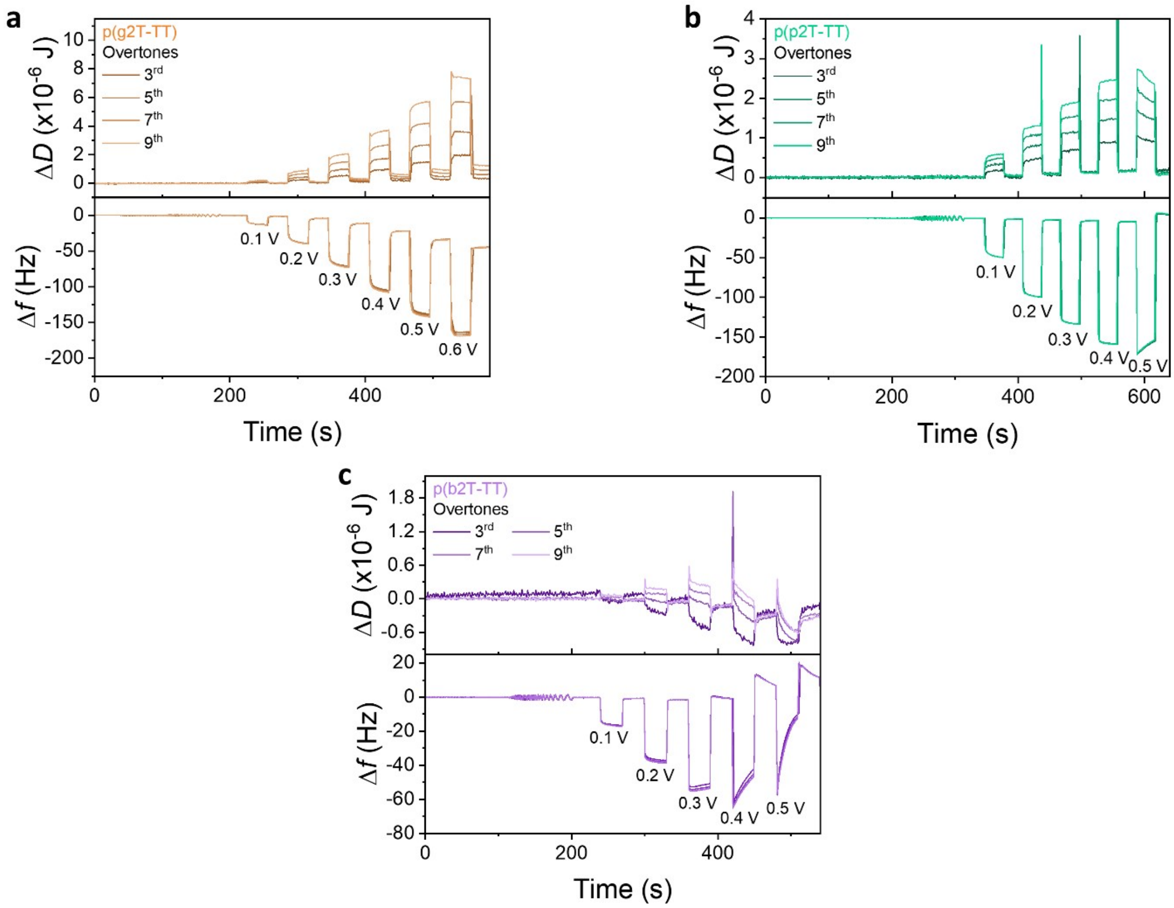

Fig S38 Frequency and dissipation changes during electrochemical doping/dedoping cycles for (a) p(g2T-TT), (b) p(p2T-TT), and (c) p(b2T-TT).

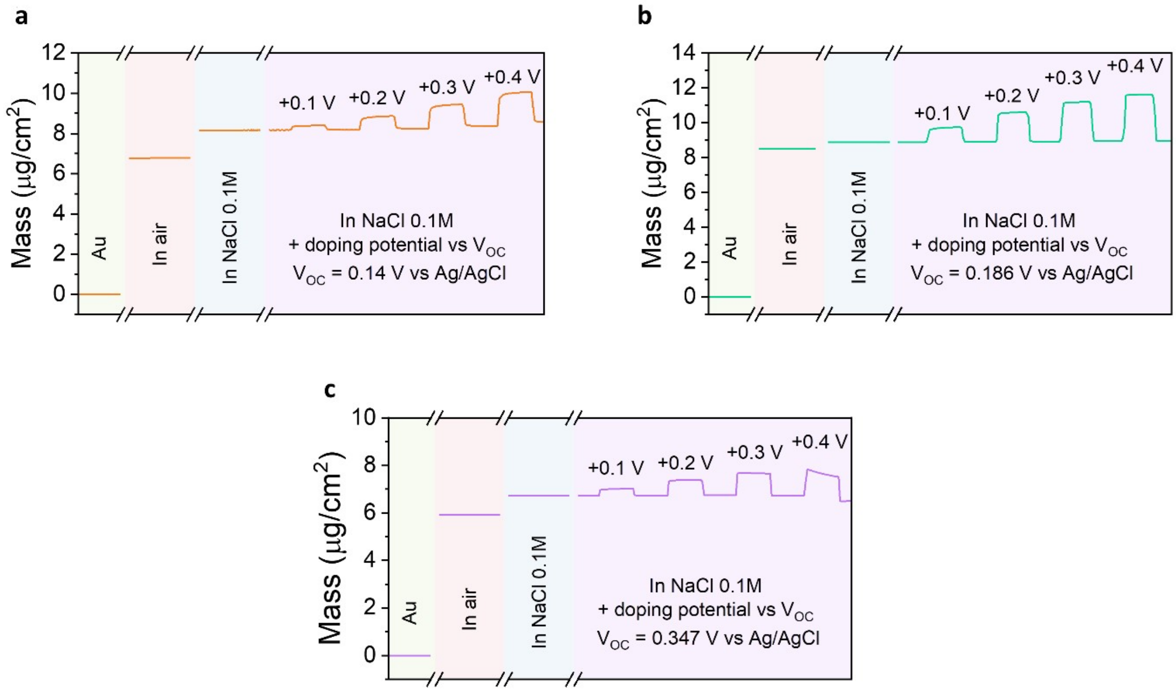

Fig S39 Mass changes of the films upon electrochemical doping for (a) p(g2T-TT), (b) p(p2T-TT), and (c) p(b2T-TT).

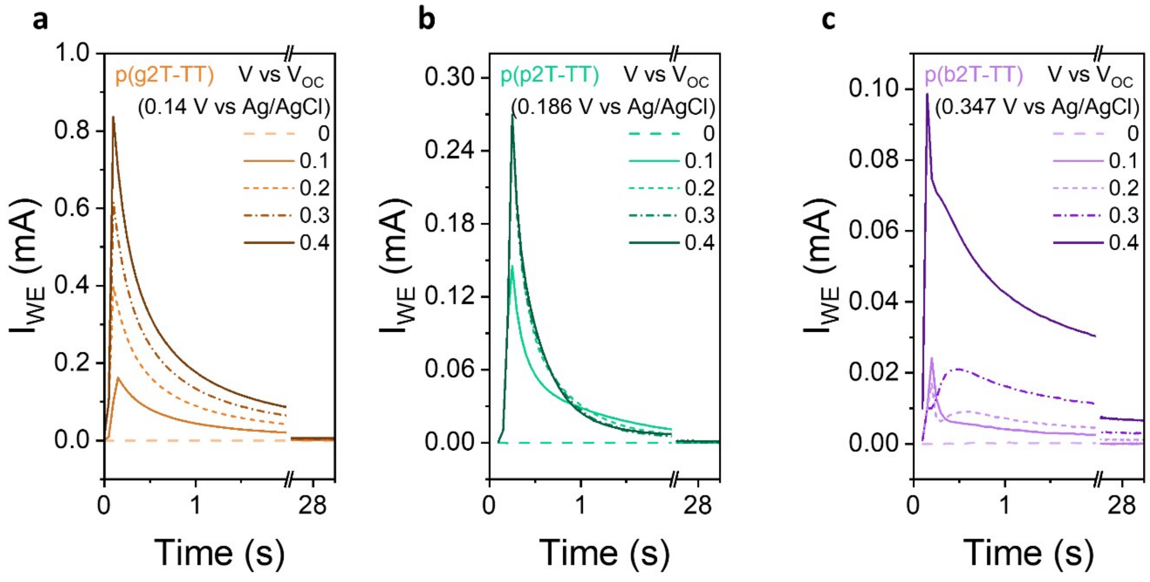

Fig S40 Current vs time profiles recorded during the eQCM-D measurements a) p(g2T-TT), b) p(p2T-TT), and c) p(b2T-TT).

11. References

1 C. M. Cardona, W. Li, A. E. Kaifer, D. Stockdale and G. C. Bazan, *Adv. Mater.*, 2011, **23**, 2367–2371.

2 I. Reviakine, D. Johannsmann and R. P. Richter, *Anal. Chem.*, 2011, **83**, 8838–8848.

3 A. H. Jahromi, Y. Fu, K. A. Miller, L. Nguyen, L. M. Luu, A. M. Baranger and S. C. Zimmerman, *J. Med. Chem.*, 2013, **56**, 9471–9481.

4 E. C. Knuf, J.-K. Jiang and M. S. Gin, *J. Org. Chem.*, 2003, **68**, 9166–9169.

5 M. Moser, L. R. Savagian, A. Savva, M. Matta, J. F. Ponder, T. C. Hidalgo, D. Ohayon, R. Hallani, M. Reisjalali, A. Troisi, A. Wadsworth, J. R. Reynolds, S. Inal and I. McCulloch, *Chem. Mater.*, 2020, **32**, 6618–6628.

6 A. Giovannitti, I. P. Maria, D. Hanifi, M. J. Donahue, D. Bryant, K. J. Barth, B. E. Makdah, A. Savva, D. Moia, M. Zetek, P. R. F. Barnes, O. G. Reid, S. Inal, G. Rumbles, G. G. Malliaras, J. Nelson, J. Rivnay and I. McCulloch, *Chem. Mater.*, 2018, **30**, 2945–2953.

7 A. Giovannitti, R. B. Rashid, Q. Thiburce, B. D. Paulsen, C. Cendra, K. Thorley, D. Moia, J. T. Mefford, D. Hanifi, D. Weiyuan, M. Moser, A. Salleo, J. Nelson, I. McCulloch and J. Rivnay, *Adv. Mater.*, 2020, **32**, 1908047.